Development of a Monolithic-like Precast Beam-Column Moment Connection: Experimental and Analytical Investigation

Mehmet Senturk [1,3,*], Selim Pul [1], Alper Ilki [2], Iman Hajirasouliha [3]

[1] Department of Civil Engineering, Karadeniz Technical University, Trabzon, Turkey
[2] Department of Civil Engineering, Istanbul Technical University, Istanbul, Turkey
[3] Department of Civil & Structural Engineering, The University of Sheffield, Sheffield, UK
* Corresponding Author: e-mail: mehmet.senturk@sheffield.ac.uk

Abstract: This study aims to develop a novel monolithic-like precast beam-column connection for reinforced concrete (RC) structures. The proposed connection system has several advantages such as rapid assembly and disassembly, reusability, and being replaceable if damaged during an earthquake event. An experimental investigation was first carried out to determine the seismic performance of the proposed connections. In total, six full-scale precast and monolithic T-shape beam-column connection specimens with different reinforcement ratios, specimen dimensions and detailing were tested under displacement controlled cyclic loading, while the axial load on the column was kept constant. The cyclic behaviour, curvature distribution, failure mode, energy dissipation capacity and ductility of the specimens were obtained using the experimental outputs. Detailed non-linear finite element (FE) models were then developed using ABAQUS. It is shown that the FE models can accurately predict the overall performance of the precast connections in terms of initial stiffness, lateral load-bearing capacity and post peak behaviour. The results indicate that, in general, the precast connections exhibited considerably higher (up to 34%) ductility and ultimate drift ratio (deformability) compared to similar monolithic connections. For the same drift ratio, monolithic connections exhibited slightly higher (on average 10%) energy dissipation capacity, while the precast connections generally dissipated higher energy at their ultimate point (post-peak lateral drift corresponding to 15% loss in lateral strength). It is demonstrated that the monolithic-like precast connections can satisfy the ACI 318-14 acceptance criteria, while they also sustain the ASCE 41-17 Collapse Prevention (CP) limits. Therefore, the proposed connection system is considered to be suitable for RC structures in seismic regions.

Keywords: Precast Concrete; Monolithic-like Connections; Cyclic Loading; Seismic Performance; Ductility

1. Introduction

As a result of population growth and increasing demand for higher standards, the modern construction industry is facing new challenges to develop more efficient and sustainable structural systems to comply with the requirements such as resilience, cost efficiency, fast construction and ease of off-site manufacturing [1]. Compared to conventional cast-in-situ reinforced concrete (RC) structures, the precast concrete elements are fabricated in the plant, resulting in several advantages such as better material quality, precise geometry and lower cost [2, 3]. On the other hand, shrinkage and creep in precast elements mainly occur before fabrication, which can reduce in-service concrete stresses [3]. Using precast construction technology also decreases the occupational health and safety risks by minimising the labour work at site [4, 5]. Precast structures generally provide cost-efficiency and fast construction due to mass production and no need for curing on site after assembly of the members [5-7]. Moreover, using precast elements can minimise construction waste compared to conventional construction methods [8].

The connections between the precast members are usually the most vulnerable parts of the structures, especially under extreme load events [9]. Due to this limitation, precast structures are not extensively used in seismic zones [10, 11]. While precast connections are generally categorised into dry and wet connections [12], Ozturan et al. [13] classified them into three main categories including wet connections with cast-in-place concrete, composite wet connections with welding, and dry connections with bolts. To evaluate the structural performance of these systems, Zhou et al. [14] developed simplified bond stress models for more accurate prediction of the structural performance of reinforced concrete structures in both pre- and post-yield phases. In another relevant study, a new automated detection method was suggested by Chen et al. [15] for engineering structures with cyclic symmetries.

French et al. [16] investigated experimentally the cyclic behaviour of four different types of wet and dry precast connections, which in general demonstrated the adequate strength and ductility of both types of connections. In another study, Vidjeapriya and Jaya [17] suggested two new precast connection systems using simple mechanical components, and showed the efficiency of their proposed connections through cyclic loading tests. It was observed that their proposed precast connections could provide an energy dissipation capacity and ductility level comparable with similar monolithic connections. Similarly, Li et al. [18] developed a new type of hybrid-steel precast beam-column connection, which was shown to have an adequate ductile behaviour under seismic loading. Using energy absorbing ductile connectors, Englekirk [19, 20] proposed a precast moment resisting connections for high seismic zones. The results of their studies demonstrated the good performance of the proposed connection compared to conventional cast-in-place systems.

More recently, Lago et al. [21] demonstrated the efficiency of an innovative dry-assembled precast structural system with special mechanical connection devices.

Choi et al. [22] developed a wet precast column-beam connection system by using steel plates inside the connection to achieve the continuity of the connection and improve the structural performance. A new ductile precast beam-column connection was also proposed by Parastesh et al. [23] for moment-resisting frames in high seismic regions. Based on a series of cyclic loading tests, it was concluded that the proposed precast connections could provide sufficient flexural strength and considerably higher ductility and energy dissipation capacity compared to similar monolithic connections. Experimental tests conducted by Ertas et al. [13] on four full-scale connections including cast-in-place precast connection, composite precast connection with welding, bolted precast connection and monolithic connection concluded that only the bolted precast connection could be considered suitable for high seismic applications. In a follow-up study, Ozden and Ertas [24] investigated experimentally the cyclic behaviour and flexural capacity of precast beam-column connections with different mild steel reinforcement ratios. It was demonstrated that by increasing the reinforcement ratio, the energy dissipation capacity of the connections increases, while the ductility is not considerably affected. Aninthaneni and Dhakal [25] presented a new concept for demountable precast connections that could be reused after the effective life of the building, leading to considerable savings in the material waste and energy associated with the demolition of the structure. A column-to-column connection system was also proposed by Nzabonimpa and Hong [26], in which metal filler plates were used to create a rigid joint. The efficiency of the proposed system was investigated experimentally and analytically and the results were used to develop practical design recommendations. More recently, Chen et al. [27] developed a novel assembling method for precast reinforced concrete shear walls using bundled connections. It was shown that the proposed system can prevent cracking at the bottom of the shear walls and provide a satisfactory structural performance and failure mode.

While most of the existing moment-resisting precast connections were shown to have acceptable flexural strength, energy dissipation capacity and ductility, they do not generally behave at the same level of similar monolithic connections. Moreover, typical moment-resisting precast connections generally require complex geometry or special assembly techniques such as post-tensioning, welding or minor casting. They may also change the typical failure mode of the connections, and therefore, require more sophisticated design approaches to obtain the target performance level. This study aims to develop a new monolithic-like precast beam-column moment connection by using a novel plate anchorage technique. Compared to most conventional precast connections, the proposed system can be quickly fabricated, it is easy to assemble and disassemble, and can be replaced if it is

damaged under an extreme load condition (e.g. strong earthquake). Moreover, the proposed monolithic-like precast connection does not considerably change the failure mode and overall behaviour of the connection, and hence can be designed based on traditional design approaches. In this study, the performance of the developed connection is demonstrated through experimental tests and analytical investigations on six full-scale specimens as will be explained in the following sections.

2. Concepts of the Proposed Monolithic-like Precast Connection System

The general concept of the proposed connection system is given in Fig. 1-a. The main aim is to develop a precast connection that behaves the same way as monolithic connections by preventing damage in the connection component (i.e. plates, bolts, anchorage rods). In the compression zone of the beam-column interface, the utilised plates can directly transfer the compressive loads between the elements. For transferring the loads in the tension zone, an innovative detailing is used between the longitudinal reinforcement of the beam and the anchorage of the column surface plate (see Fig. 1-b). In the proposed system, the anchorage of the beam end-plate to the beam is provided through longitudinal reinforcement bars with rivet heads, which are produced through regular reinforcement steel rebar using a hot forging process (see Fig. 2-a). The hot forging process is a production method for shaping the metals using localized compression forces at high temperature (forging temperature). It should be noted that to have a plain surface after the rivet head bars are in place, the beam end-plate is drilled as shown in Fig. 2-b as a part of the offsite production process. The beam end-plate is connected to the column surface plate by using high-strength bolts (see Fig. 1). Fig. 1-b illustrates how the bending moment is transferred from beam to column elements in the proposed connection system. The load transfer mechanism among the rivet head rebar, the beam end-plate and the column surface plate is shown in Fig. 2-c and Fig. 2-d in case of compression and tension, respectively. In the tension zone, the tensile force of the longitudinal reinforcement transfers through the rivet head rebar, beam end-plate, high-strength bolts, high nuts located on the column surface plate, and anchorage of the column. In the compression zone, the compression is transferred through the concrete and the rivet head rebar of the beam, beam end-plate, column surface plate, and concrete surface of the column. As mentioned above, using this detailing ensures that the dominant failure mode, the distribution of damage, and plastic deformations would be close to those of an identical monolithic connection.

It should be noted that the traditional construction techniques that are generally used to assemble precast systems (e.g. formwork, steel works, concrete casting and curing in situ) can be very time-consuming. Using the precast connection system proposed in this study eliminates the need for in-

situ concrete curing as structural members are directly connected through pre-tensioned bolts using a novel plate anchorage technique. This feature can considerably increase the construction speed, and therefore, reduce the construction costs compared to the traditional methods.

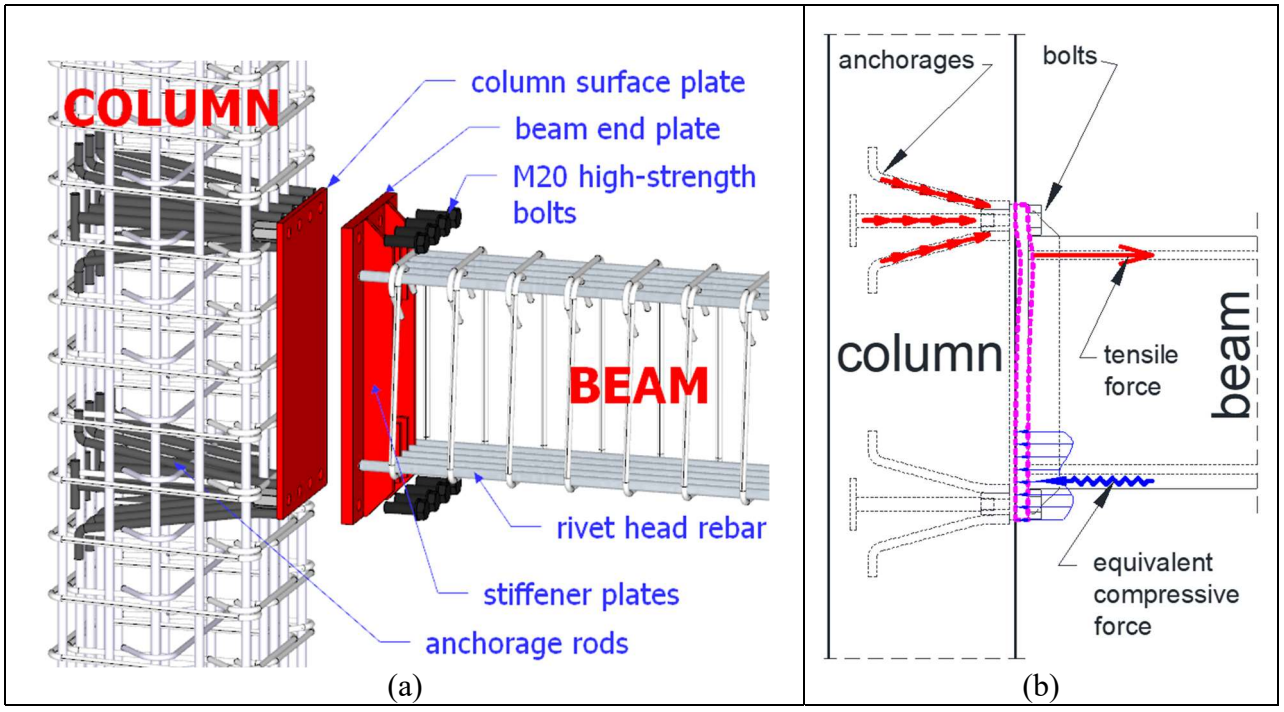

Fig. 1. General concept of the proposed connection system; (a) Geometry of beam to column connection; (b) General load transfer mechanism

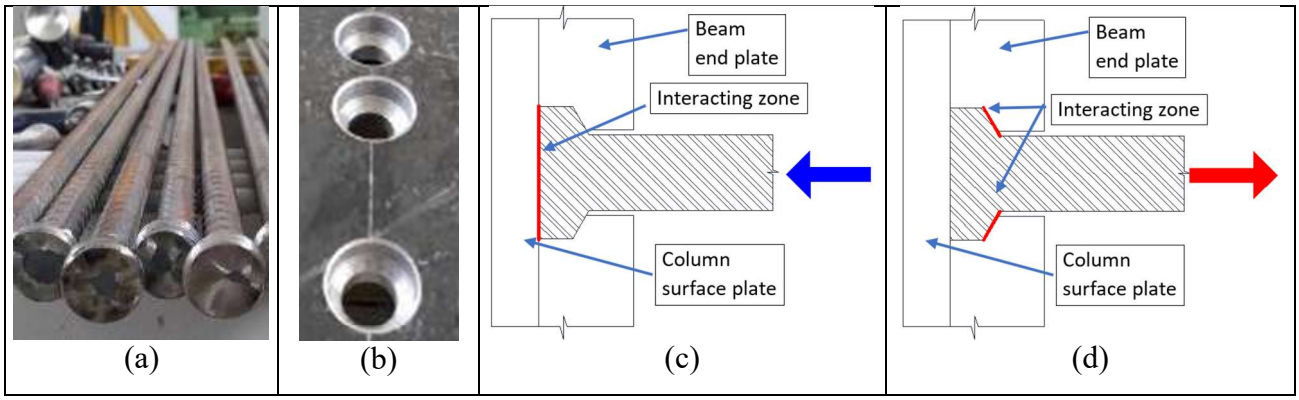

Fig. 2. Details of rivet head rebar; (a) Rivet head rebar; (b) Hole for rivet head rebar; (c) Load transfer mechanism in compression; (d) Load transfer mechanism in tension

3. Test specimens

3.1. Geometry and reinforcement detailing

In this study, six full-scale precast and monolithic T-shape connection specimens were manufactured and tested under cyclic loading to examine the efficiency of the proposed connection system. The cross-sectional dimensions and the reinforcement details for the beam and column

elements of the tested specimens are listed in Table 1. It can be seen that, for better comparison, precast and monolithic connections use the same reinforcement ratios in the beam and column elements. To investigate the effect of different design approaches, CB1 and CB2 specimens were designed based on "strong-beam and weak-column" and "strong-column and weak-beam" concepts, respectively.

As shown in Table 1, CB1 specimens have lower beam and column longitudinal reinforcement ratios compared to the CB2 specimens, while they have lower transverse reinforcement ratio in the column elements. A stiffer beam end-plate system is also used for the CB2 specimens. CB2 specimens have 1.0 m and 2.0 m beam length to obtain different types of structural behaviour at the connection zone. The specimens with 1.0 m beam length have larger bending moment over shear force ratio than the specimens with 2.0 m beam length, and hence they are likely to fail due to shear. It should be noted that CB1 specimens have inadequate shear reinforcement in their panel zone to highlight the effects of the proposed connection system on the behaviour of the panel zones with different reinforcement details representing both standard and substandard designs. It will be discussed in the following sections that the anchorage system and the column surface plate used in the proposed precast connection could considerably improve the shear behaviour of the connection panel zona and change the failure mechanism.

In the identification code adopted in this study, the first number after CB refers to the type of the detailing and the reinforcement ratios of the beam and column elements. The "Mon" and "Pre" terms represent monolithic and precast connections, respectively. The number at the end of the identification code refers to the length of the beam element (1.0 m or 2.0 m). For example, CB2-Mon-1 specimen is a monolithic connection with 1.0 m beam length, stiffer beam end-plate system, and higher longitudinal and transverse reinforcement ratios. Fig. 3 shows the geometric and reinforcement details of this specimen (CB2-Mon-1). The general views of CB2 specimens with 1.0 m and 2.0 m beam length are also illustrated in Fig. 4.

Table 1. Details of the tested precast and monolithic connections

No.	Specimen Name	Connection Type	Column			Beam			
			Cross-Section (mm)	Longitudinal Reinforcement (Ratio)	Transverse Reinforcement (mm)	Cross-Section (mm)	Span (mm)	Longitudinal Reinforcement (Ratio)	Transverse Reinforcement (mm)
1	CB1-Mon-1	Monolithic	300×300	8Ø14 (%1.4)	Ø8/80	250×400	1000	10Ø14 (%1.5)	Ø8/100
2	CB1-Pre-1	Precast	300×300	8Ø14 (%1.4)	Ø8/80	250×400	1000	10Ø14 (%1.5)	Ø8/100
3	CB2-Mon-1	Monolithic	400×400	16Ø16 (%2)	2Ø8/100	250×400	1000	10Ø16 (%2)	Ø8/100
4	CB2-Pre-1	Precast	400×400	16Ø16 (%2)	2Ø8/100	250×400	1000	10Ø16 (%2)	Ø8/100
5	CB2-Mon-2	Monolithic	400×400	16Ø16 (%2)	2Ø8/100	250×400	2000	10Ø16 (%2)	Ø8/100
6	CB2-Pre-2	Precast	400×400	16Ø16 (%2)	2Ø8/100	250×400	2000	10Ø16 (%2)	Ø8/100

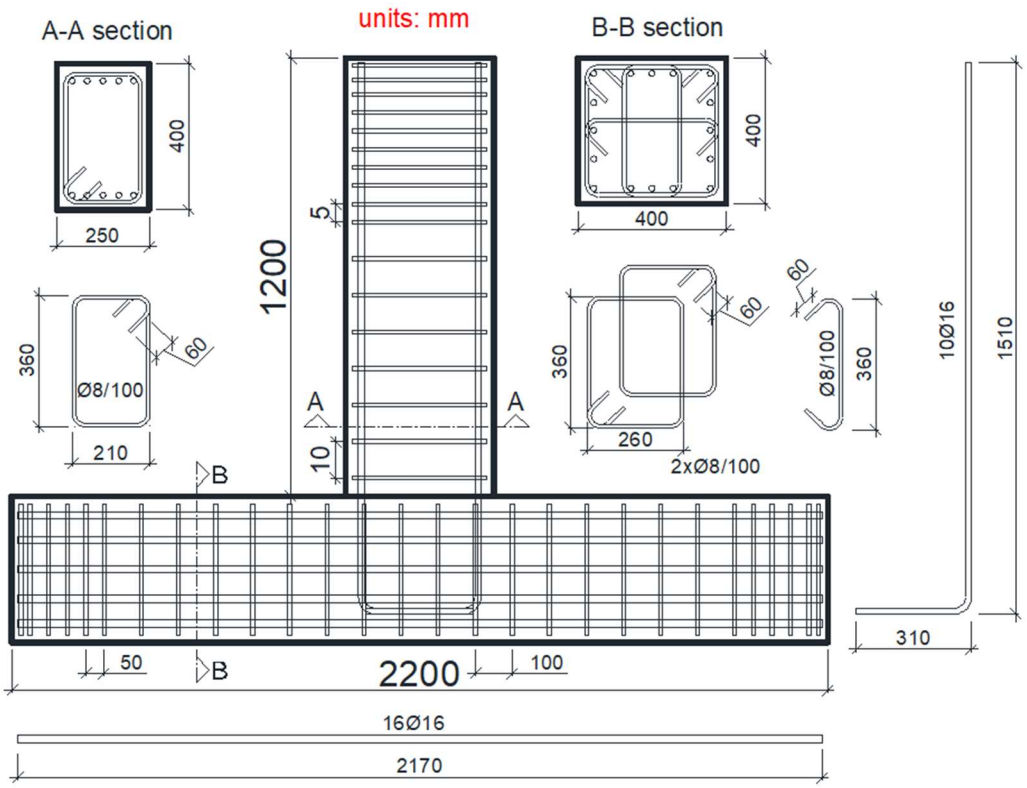

Fig. 3. Geometric and reinforcement details of the test specimen CB2-Mon-1

(a) (CB2-Mon-1, CB2-Mon-2) (b) (CB2-Pre-1, CB2-Pre-2) (c) Close up view of precast connection

Fig. 4. General view of CB2 monolithic and precast specimens with 1.0 and 2.0 m beam length and the close-up view of the adopted precast connection

Fig. 5 and Fig. 6 show the details of the connection plates used for CB1 and CB2 precast specimens, respectively. Since the beam elements are designed to resist both seismic and gravity loading conditions (both cases create bending moment in the same axis), vertical stiffener plates were placed on the beam end-plate of both CB1 and CB2 specimens. To transfer bending moments from the beam to the column, high strength bolts were located on the top and bottom edges of the connection plates. The bolts and nuts in the proposed connection system were designed to remain in their elastic zone when the specimen fails. As discussed before, for the anchorage of the beam end-

plate to the beam element, the longitudinal reinforcement bars of the beam with rivet head were used (see Fig. 2). For the anchorage of the column surface plate to the column in the CB1 precast specimen, welded anchorage rods were used as shown in Fig. 5-b.

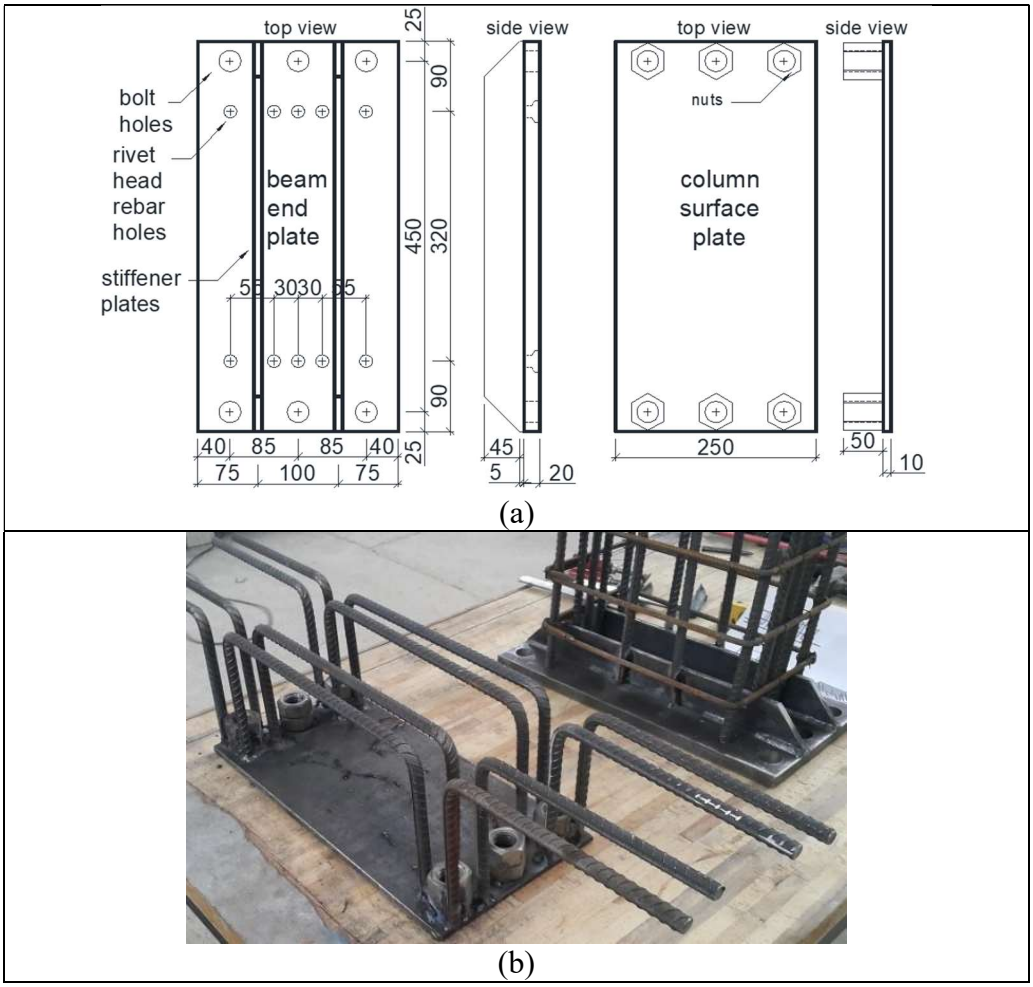

Fig. 5. Details of connection plates of CB1-Pre-1 specimen; (a) Geometry of beam end-plate and column surface plate; (b) General views of the beam end-plate and column surface plate

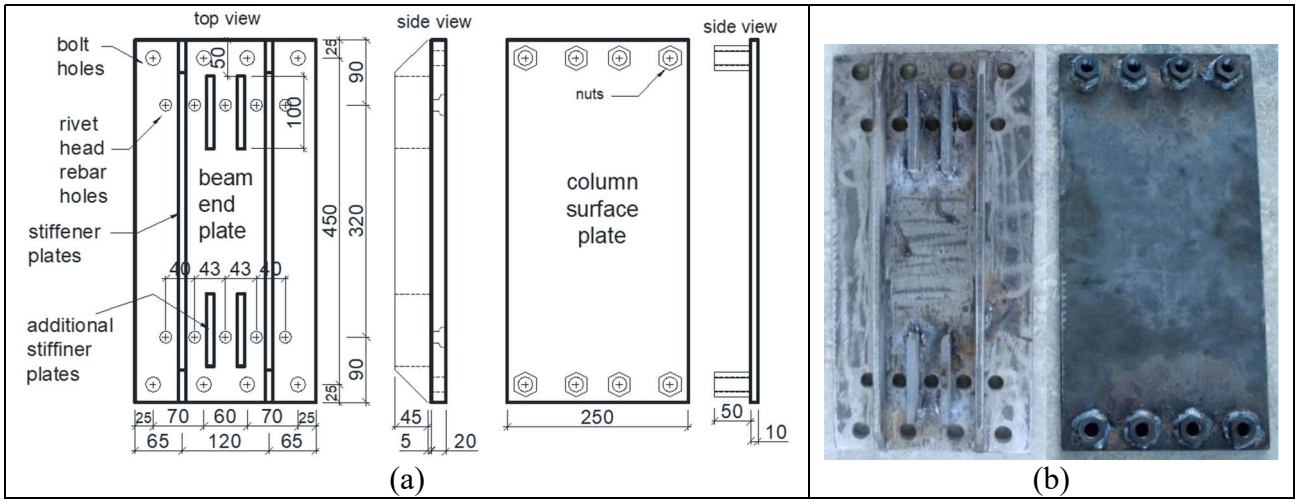

Fig. 6. Details of connection plates used for CB2-Pre-1 and CB2-Pre-2 specimens; (a) Geometry of beam end-plate and column surface plate; (b) General views of the beam end-plate and column surface plate

Since the longitudinal reinforcement ratios of the columns in CB2 specimens were higher than those of CB1 specimens, the anchorage system was improved to take smaller space for easy installation and casting. For this purpose, anchorage rods with threaded ends as well as additional welded anchorage rods were utilised. Fig. 7 shows the anchorage details for the column surface plate used for CB2-Pre-1 and CB2-Pre-2 specimens. It should be noted that the utilised anchorage details were over-designed to prevent the anchorage failure during the tests.

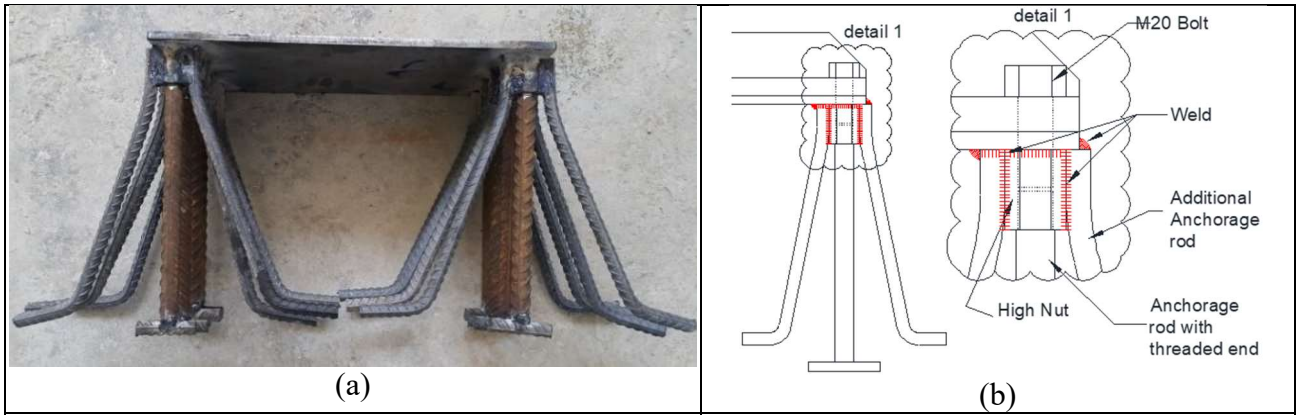

Fig. 7. Anchorage details of the column surface plate used for CB2-Pre-1 and CB2-Pre-2 specimens; (a) Details of column surface plate; (b) Details of anchorage, bolt and fastening

3.2. Material properties

3.2.1. Reinforcing bars

Tensile tests were carried out on both regular bars and rivet head rebars using a Universal Testing Machine (Fig. 8-a), to ensure the heating process during the fabrication of the rivet head rebar does not considerably change its mechanical characteristics. Since only the end part of the rebar was heated, the failure point was always outside the rivet head zone (or heated zone) as shown in Fig. 8-b. This means that the local heating process did not affect the overall behaviour of the rivet head rebar in the proposed connection system.

The stress-strain relationships of regular and rivet head rebars are compared in Fig. 8-c (average of three samples). In general, the results indicate that the adopted heating process did not considerably change the characteristics of the rebars. The average yield and ultimate strengths of regular rebar was obtained as 491 MPa and 618 MPa, respectively. For the rivet head rebar (i.e. after the heating process), the average yield and ultimate strength values changed to 471 MPa and 598 MPa, respectively. The modulus of elasticity, yield strain, hardening strain and ultimate strain of both regular and rivet head rebar were almost similar (see Fig. 8-d).

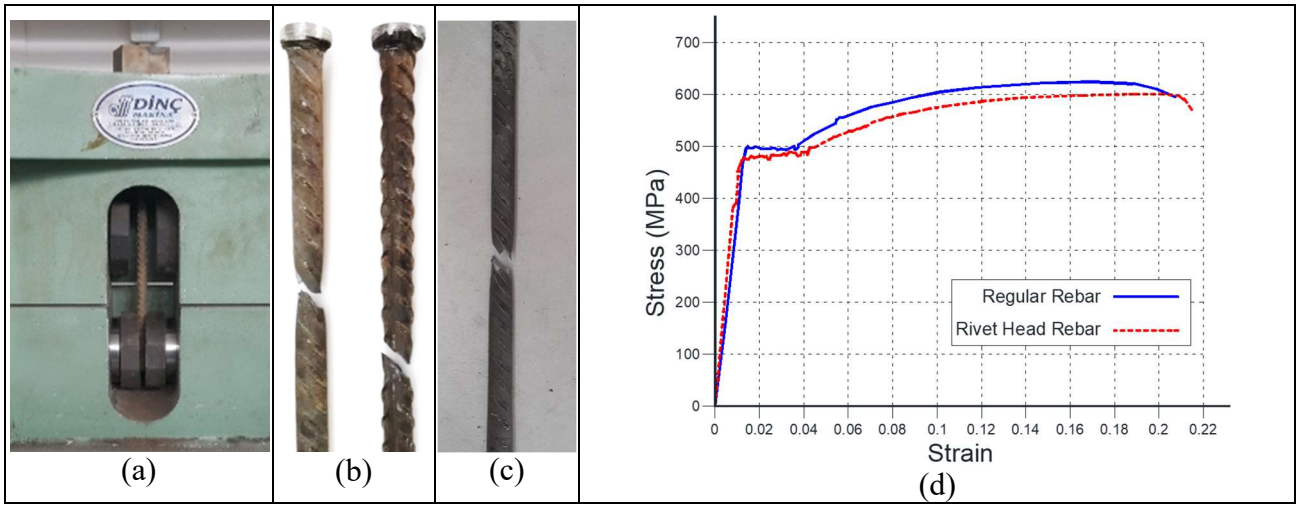

Fig. 8. (a) Tensile test machine; (b) Failure mode of rivet head rebar; (c) Failure mode of regular rebar; (d) Stress-strain relationships of regular and rivet head rebars

3.2.2. Concrete

The concrete mix-proportions used for CB1 and CB2 specimens are presented in Table 2. In order to obtain the compressive strength of the concrete, load controlled compression tests were conducted on 150 mm cubic specimens using a 2500 kN capacity Universal Testing Machine. The loading rate was set to be 0.4 MPa/s [28]. The calculated compressive strength values (average of three tests for each case) are listed in Table 3.

Table 2. Concrete mix-proportions

Specimens	D_{max}* mm	Water/Cement Ratio	Cement kg/m^3	Cement type	Mixing Water kg/m^3	Total Water (with saturated water) kg/m^3	Total aggregate kg/m^3	Super Plasticiser kg/m^3
CB1 Group	22	0.5	400	Grade 32.5	200	217	1735	4 (%1.7)
CB2 Group	22	0.5	285	Grade 42.5	143	163	2000	3.4 (%1.4)

*Maximum aggregate size

Table 3. Concrete compressive strength values

Specimens	Cube compressive strength at 28 days (MPa)	Cube compressive strength at test day (MPa)
CB1 Group	30.0	43.2
CB2 Group	42.2	53.4

3.2.3. Bolts and Nuts

For the CB1 specimens, 8.8 grade high strength M27 bolts (27 mm diameter) were used. To design the connections, the theoretical yield and ultimate stress of the M27 bolts were taken as 640 MPa, 800 MPa, respectively. The core area of M27 bolts was considered to be 419 mm^2.

For the CB2 specimens, 10.9 grade high strength M20 bolts (20 mm diameter) were utilised. To obtain the strength and failure mechanism of M20 bolts, tensile tests were carried out using both 6.8 grade regular strength and 10.9 grade high strength nuts. In case of regular nuts, the failure mode

was observed as shearing the threads of nuts (see Fig. 9-a), while in case of high strength nuts, the dominant failure mode was the rupture of the bolts (see Fig. 9-b). The theoretical yield and ultimate stress (both provided by the manufacturer) and the measured experimental rupture stress values are listed in Table 4. The core area of M20 bolts was considered to be 220 mm^2.

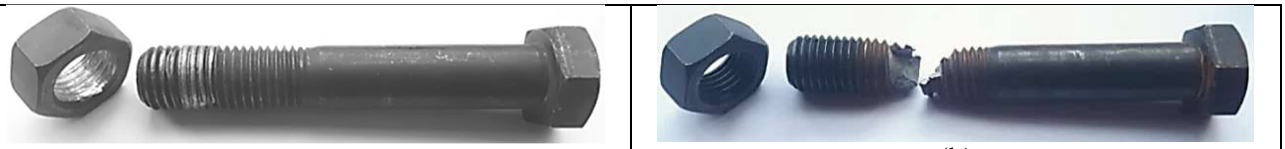

(a) (b)

Fig. 9. After test view of the bolts and nuts; (a) 10.9 grade M20 bolt + 6.8 grade nut; (b) M20 bolt + 10.9 grade nut

Table 4. Tensile test results for 10.9 grade M20 bolts with 6.8 and 10.9-grade nuts

Bolt – nut combination	Failure load (kN)	Theoretical yield stress for 10.9-grade steel (MPa)	Theoretical ultimate stress for 10.9-grade steel (MPa)	Experimental rupture stress for the bolt (MPa)	Failure mode
10.9 grade M20 bolt + 6.8 grade nut	233	900	1000	-	Shearing the thread of the nut
10.9 grade M20 bolt + 10.9 grade nut	268	900	1000	1218	Rupture of the bolt
10.9 grade M20 bolt + 10.9 grade nut	283	900	1000	1286	Rupture of the bolt

3.2.4. Plates

S235 (ST37) grade structural steel was used for the column surface plate and the beam end-plate. Invert-gas welding technique was used to weld stiffener plates and anchorage rods on the beam end-plate and column surface plate, respectively (see Fig. 5 and Fig. 6).

4. Experimental Test Setup

Fig. 10 illustrates the side view of the test setup (specimens with 1.0 m beam length) and the measurement system used in this study. For the specimens with 2.0 m beam length, the location of the hydraulic actuator was raised by 1.0 m. During the tests, a constant axial load was applied to the columns. The axial load was chosen as 10% of the load-bearing capacity of each column calculated by using the average compressive strength of concrete and the gross area of the column cross-section. It can be noted from Fig. 10-a that in the adopted test set up, the column element was set to be horizontal while the beam element was placed vertically. This arrangement could simplify the detailing required to apply the axial load to the column and help to maintain the load level during the cycling loading tests. Due to the difficulty of placing hinges and the vertical supports at the column ends in the same vertical axis, these supports were designed to have a small spacing between the hinges and the vertical support. As the expected rotation values at the column ends

were very small, it could be assumed that the spacing between the hinge and the vertical support had a negligible effect on the rotational behaviour of the column.

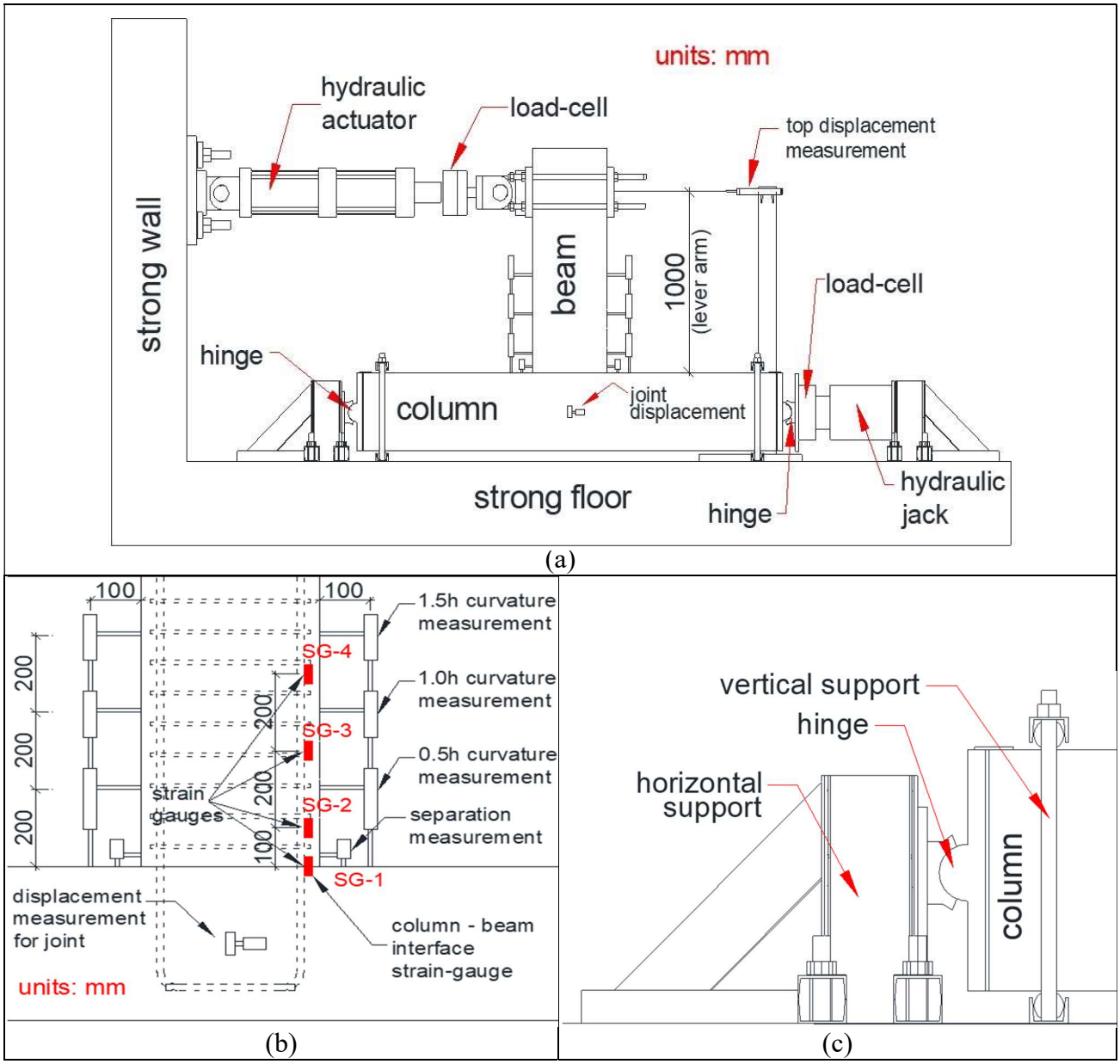

Fig. 10. (a) Experimental test setup; (b) Details of the displacement transducers and strain-gauges; (c) Details of the column support

For the curvature measurements, six displacement transducers were located at 200 mm (0.5h), 400 mm (1.0h) and 600 mm (1.5h) levels from the column surface as shown in Fig. 10-b (h is the height of the beam cross-section). Four strain-gauges were also mounted on the longitudinal reinforcement bars of the beam elements to monitor the yielding zone in the connections (see Fig. 10-b). Subsequently, displacement controlled quasi-static reversed cyclic lateral loading tests were performed, while the axial load was kept constant on the column. The lateral loading protocol given in FEMA-461 [29] was applied to the tip of the beam element (see Fig. 10-a). Fig. 11 shows the

loading protocol used in this study. The selected loading protocol has two cycles for each displacement level. The lateral loading was continued until the failure point.

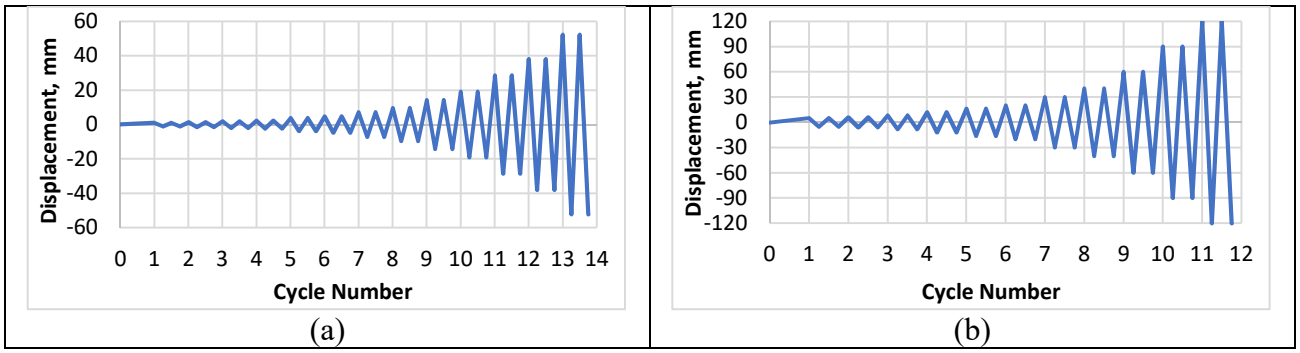

Fig. 11. Lateral loading protocol, adopted from FEMA-461 [29] (a) loading protocol for the specimens with 1.0 m beam; (b) loading protocol for the specimens with 2.0 m beam

It should be noted that the failure of the connections can be defined in different ways such as reaching the maximum concrete compression strain, significant loss in the load-bearing capacity, and fracture or buckling of the element [30]. In this study, 20% drop in maximum load-bearing capacity of the connections or buckling of the longitudinal reinforcement was considered as the failure point (whichever occurs first).

5. Experimental Results

The connections were subjected to cyclic displacement reversals shown in Fig. 11 up to the failure point. Observations and measured data from the tests were used to obtain cyclic behaviour, curvature distribution, failure mode, energy dissipation and ductility of the monolithic and precast connection specimens as will be discussed in the following sections.

5.1. Cyclic behaviour

To obtain the cyclic behaviour of the connections, the relative top displacement of the beam (calculated by subtracting the displacement of the beam-column interface from the beam top displacement) was plotted against the lateral load applied by the actuator. The lateral displacement of the beam-column interface was assumed to be equal to the joint displacement as shown in Fig. 10-a. The drift ratios were then calculated using the following equation:

$$\Delta = \delta / L \quad (1)$$

where Δ is the drift ratio, δ is the relative top displacement of the beam, and L is the lever arm length. The lever arm length was calculated from the beam-column interface to the loading point.

The cyclic behaviour curves for CB1 monolithic and precast specimens are compared in Fig. 12. The initial stiffness of the monolithic and precast specimens was calculated as 25.98 kN/mm and 26.73 kN/mm, respectively. It can be seen that both specimens have almost similar initial stiffness

values. However, the stiffness of the monolithic specimen suddenly decreased at 1 % drift ratio, while the precast specimen exhibited a gradual stiffness degradation up to 2 % drift ratio. This different behaviour is mainly attributed to the fact that the failure mode in the CB1 monolithic specimen was started with flexural cracking and yielding of the longitudinal reinforcement followed by the shear failure at the panel zone. However, using the anchorage system in the precast connection could prevent the shear failure mode by increasing the shear strength of the connection zone. The failure mode of CB1 precast specimen was due to the flexural cracking and yielding of the longitudinal reinforcement followed by shear failure at the potential plastic hinge zone of the beam. This failure mechanism led to some ductile behaviour in both monolithic and precast connections as will be discussed in the following sections. The results in Fig. 12 indicate that for CB1 specimens, the precast connection resulted in around 20% higher flexural capacity. This can be also explained by the different shear failure modes observed in these two specimens.

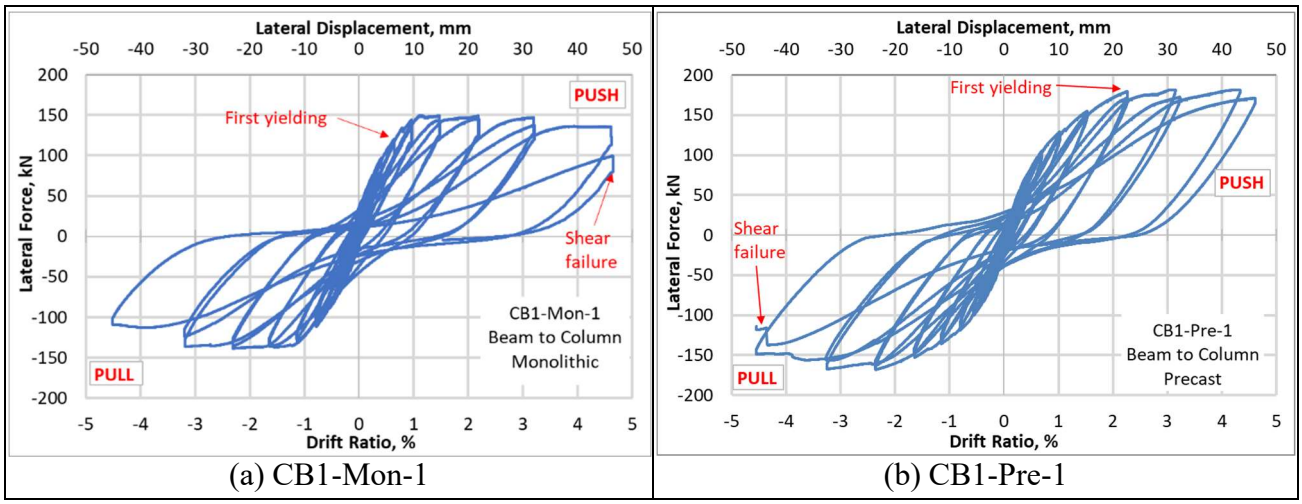

(a) CB1-Mon-1 (b) CB1-Pre-1

Fig. 12. Cyclic behaviour of CB1 specimens

The test results for CB2 specimens with 1.0 m and 2.0 m beam elements are shown in Fig. 13 and Fig. 14, respectively. The initial stiffness of CB2-Mon-1 and CB2-Pre-1 were calculated as 35.41 kN/mm and 30.66 kN/mm, respectively. Similarly, the initial stiffness of CB2-Mon-2 and CB2-Pre-2 were estimated to be 5.03 kN/mm and 5.10 kN/mm, respectively. The results confirm that the initial stiffness of CB2 precast connections were in general very close to those of their monolithic counterparts. It can be also seen that the detailing used for the CB2 precast connections did not significantly influence the overall response and capacity of the connections (see Fig. 6).

It is observed that the monolithic specimens with 1.0 m and 2.0 m beam length reached 3% and 4.5% drift ratio at the failure point, respectively. For precast specimens, these drift limits increased to 4.5% and 6%, respectively. This implies that, compared to their monolithic counterparts, the

precast specimens have considerably higher deformability (up to 34%) without losing their load-bearing capacity. This will be discussed in more detail in the following sections.

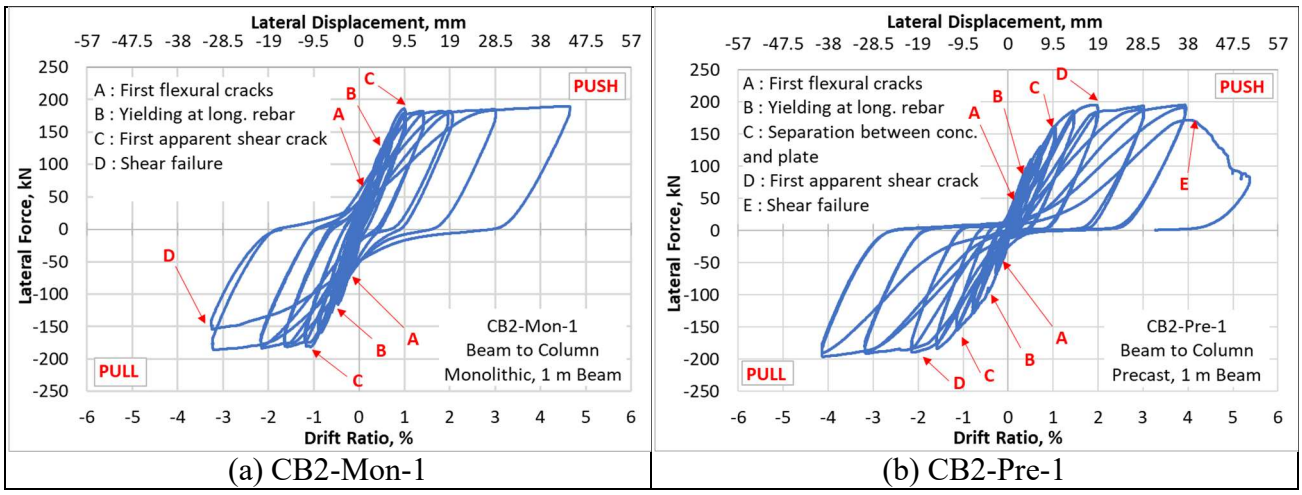

(a) CB2-Mon-1 (b) CB2-Pre-1

Fig. 13. Cyclic behaviour of CB2 specimens with 1.0 m beam length

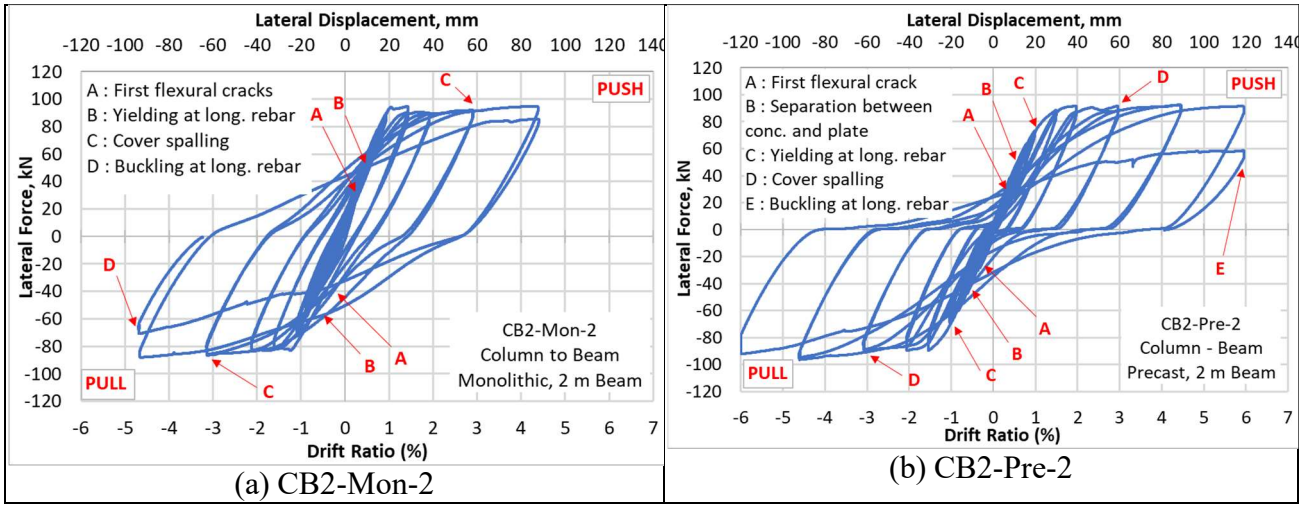

(a) CB2-Mon-2 (b) CB2-Pre-2

Fig. 14. Cyclic behaviour of CB2 specimens with 2.0 m beam length

According to ACI 318-14 [31], the beam-column connections must sustain at least 3.5% drift ratio with a maximum 25% load-bearing capacity loss. It is observed that the CB1 and CB2 specimens (except CB2-Mon-1) exhibited over 3.5% drift ratio with negligible load-bearing capacity loss (see Fig. 12Fig. 14), and therefore, can satisfy this performance criterion.

Table 5 shows the plastic rotation limits for Immediate Occupancy (IO), Life Safety (LS) and Collapse Prevention (CP) performance levels for the beam-to-column connections based on ASCE 41-17 [32]. To obtain the total rotations ($\boldsymbol{\theta_t}$) for the specimens, drift ratio is assumed as the total rotation of the beam element (i.e. $\boldsymbol{\theta_t} = \Delta$). The elastic rotations ($\boldsymbol{\theta_e}$) is the drift ratio at which the first yielding at longitudinal reinforcement occurred (see Fig. 13 and Fig. 14). Finally, the plastic rotations ($\boldsymbol{\theta_p}$) are calculated by subtracting the elastic rotations from total rotations ($\boldsymbol{\theta_p = \theta_t - \theta_e}$).

According to the failure drift ratios observed in the experimental tests, all specimens except CB2-Mon-2 reached CP seismic performance limit (see Table 5), and therefore, are suitable for RC structures in seismic regions.

Table 5. Seismic performance levels according to ASCE 41-17 [32]

Specimen	Elastic Rotation, $\boldsymbol{\theta_e}$	Plastic Rotation Limits			Total Rotation at Failure, $\boldsymbol{\theta_t}$	Plastic Rotation, $\boldsymbol{\theta_p}$	Seismic Performance Levels
		Immediate Occupancy (IO)	Life Safety (LS)	Collapse Prevention (CP)			
CB1-Mon-1	0.005	0.0015	0.0010	0.0023	0.045	0.040	CP
CB1-Pre-1	0.020				0.045	0.025	CP
CB2-Mon-1	0.005				0.030	0.025	CP
CB2-Pre-1	0.010				0.040	0.030	CP
CB2-Mon-2	0.005	0.0010	0.0020	0.0050	0.045	0.040	LS
CB2-Pre-2	0.010				0.060	0.050	CP

5.2. Average Curvature Distribution

To measure the average curvature, six displacement transducers (three at each side) were located equally spaced on the beam faces perpendicular to the loading direction (see Fig. 10-b). This measurement system was designed to divide the potential plastic hinge zone of the beam into three equal segments (0-0.5h, 0.5h-h and h-1.5h) starting from the beam-column interface, where h is the height of the beam cross section. The height of the segments was 200 mm for both CB1 and CB2 specimens. Using the measured displacements, the rotation and the average curvature of each segment were calculated geometrically as illustrated in Fig. 15.

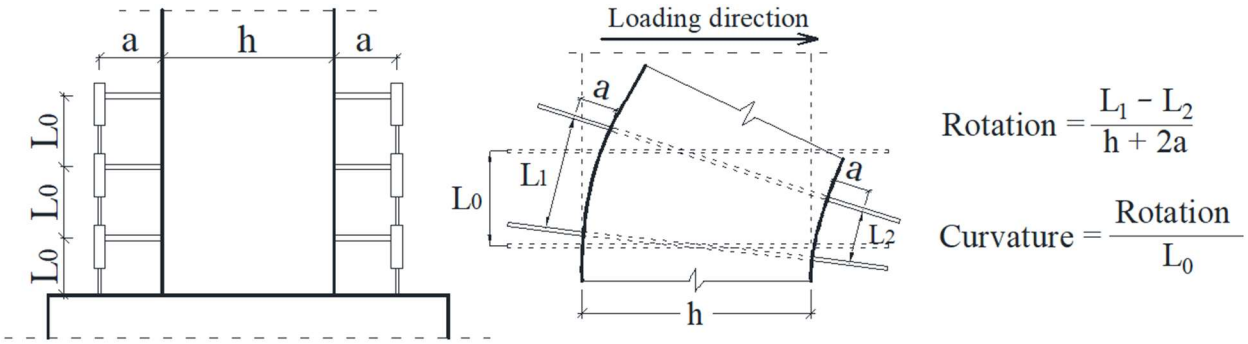

Fig. 15. Rotation and average curvature calculation

The calculated average curvature values for CB1 specimens are given in Fig. 16. For both monolithic and precast specimens, it is shown that in the lowest segment (0-0.5h) the curvature versus drift curves are almost identical (see Fig. 16-a, b). For the precast specimen (CB1-Pre-1), however, the curvature values for 0.5h-h and h-1.5h segments were approximately eight times higher than those of monolithic specimen (CB1-Mon-1) (see Fig. 16-c, d, e, f). These differences can be considered as an influence of the different failure mode observed in these two specimens as

will be discussed in the next section. It should be noted that the damage in the monolithic connection was mainly concentrated in the panel zone. Therefore, the calculated curvatures in the segments away from the connection were almost negligible.

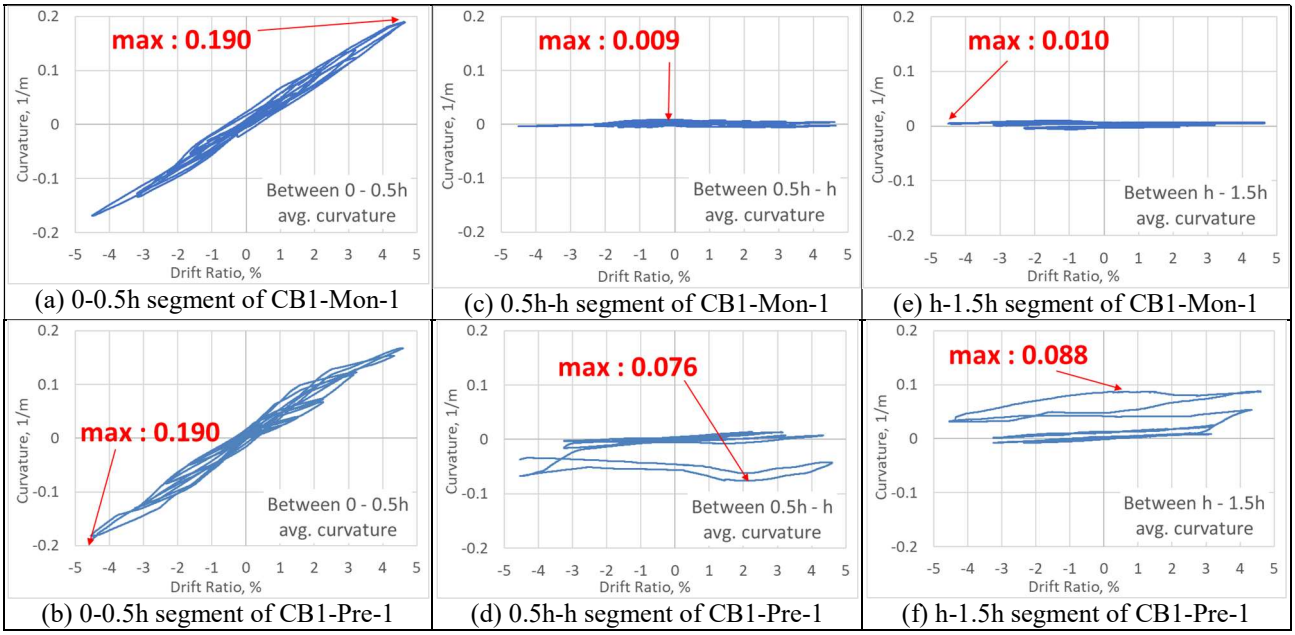

(a) 0-0.5h segment of CB1-Mon-1 (c) 0.5h-h segment of CB1-Mon-1 (e) h-1.5h segment of CB1-Mon-1

(b) 0-0.5h segment of CB1-Pre-1 (d) 0.5h-h segment of CB1-Pre-1 (f) h-1.5h segment of CB1-Pre-1

Fig. 16. Average curvatures for CB1 test specimens

Fig. 17 compares the calculated curvatures for CB2 monolithic and precast specimens with 1.0 m beam length (CB2-Mon-1, CB2-Pre-1) at different segments. It is shown that the maximum curvature values for the precast specimen were around 25% higher than the corresponding values for the monolithic connections (see Fig. 17). It can be noted that, in general, CB2 specimens with 1.0 m beam length had smaller curvature values compared to the CB1 specimens within their lowest segments. This is due to the fact that the plastic deformations were spread throughout the beam element in CB2 specimens with 1.0 m beam length for both monolithic and precast connections. As expected, for both monolithic and precast specimens, the curvature values were reduced by increasing the distance from the beam-column interface.

The calculated average curvatures for CB2 specimens with 2.0 m beam (CB2-Mon-2, CB2-Pre-2) are given in Fig. 18. It can be seen that for both monolithic and precast specimens the curvatures were similar for the first two segments (0-0.5h and 0.5h-h), while the curvature of the precast specimen for h-1.5h segment was considerably higher than the monolithic connection. Similar to the previous case, the maximum curvatures were reduced by moving away from the beam-column interface.

Based on the results, it can be inferred that the proposed precast connection system could efficiently spread the plastic deformations throughout the beam element and hence prevent localized damage (see Fig. 16, Fig. 18 and Fig. 19).

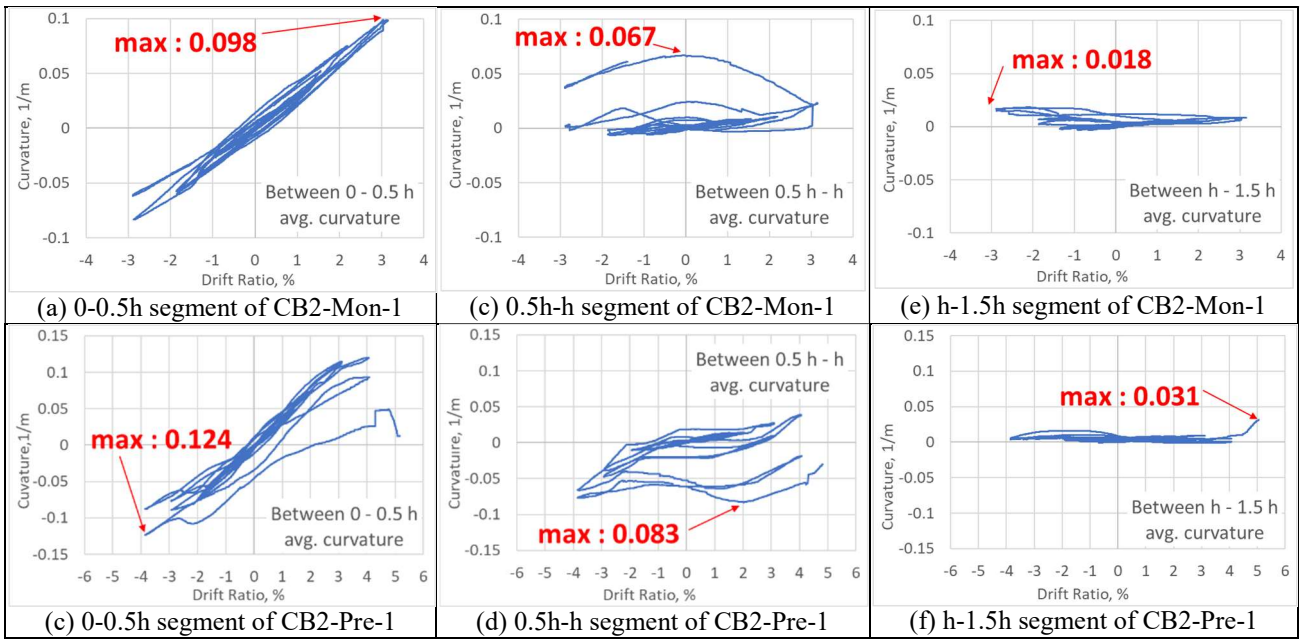

(a) 0-0.5h segment of CB2-Mon-1 (c) 0.5h-h segment of CB2-Mon-1 (e) h-1.5h segment of CB2-Mon-1

(c) 0-0.5h segment of CB2-Pre-1 (d) 0.5h-h segment of CB2-Pre-1 (f) h-1.5h segment of CB2-Pre-1

Fig. 17. Average curvatures for CB2 test specimens with 1.0 m beam length

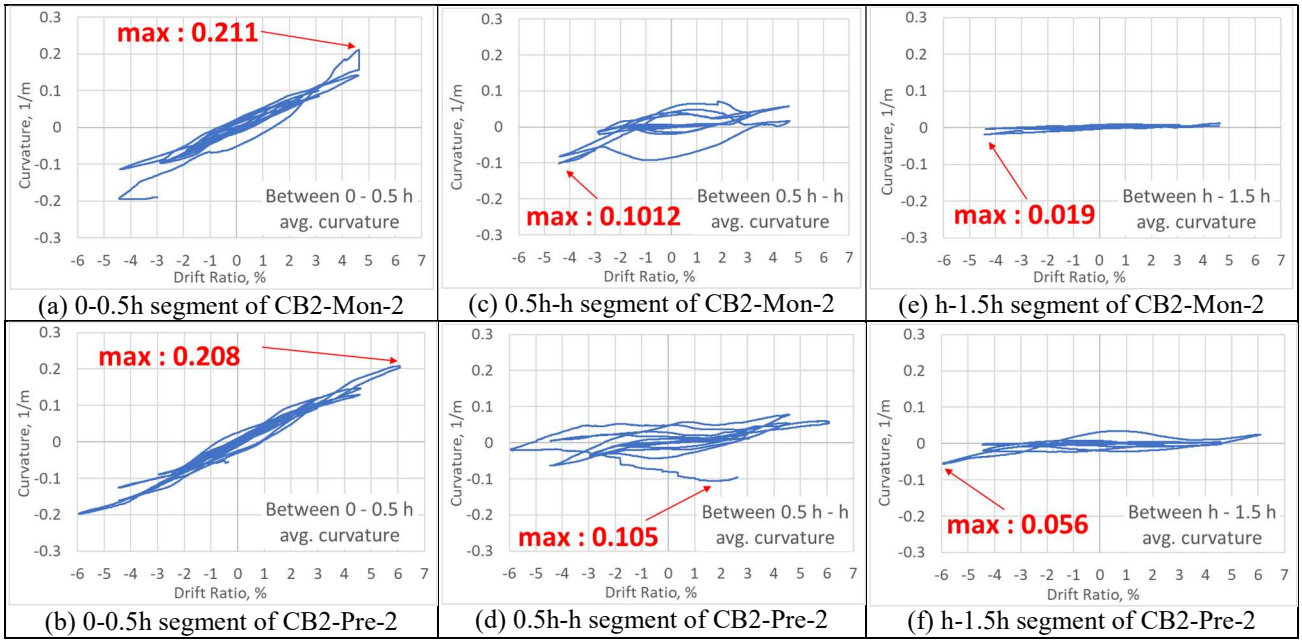

(a) 0-0.5h segment of CB2-Mon-2 (c) 0.5h-h segment of CB2-Mon-2 (e) h-1.5h segment of CB2-Mon-2

(b) 0-0.5h segment of CB2-Pre-2 (d) 0.5h-h segment of CB2-Pre-2 (f) h-1.5h segment of CB2-Pre-2

Fig. 18. Average curvatures for CB2 test specimens with 2.0 m beam length

5.3. Beam-Column Interface Separation

To obtain the crack width at the beam-column interface of the monolithic specimens and the separation between the column surface plate and the beam end-plate at the precast specimens, separation measurements were taken in this study. The separation measurement rods were anchored to the face of the beam as close to the interface as possible (see Fig. 10-b). As an example, Fig. 19 shows the separation measurement results for CB2 specimens with 1.0 m beam (CB2-Mon-1, CB2-Pre-1). Within these graphs, separation right and separation left terms represent the separation values for the right-hand and the left-hand side of the specimens according to the given drawing of

the experimental test setup (see Fig. 10-a). In Fig. 19, the negative values represent the opening (or crack growth), while the positive values indicate shortening of the beam element in compression. For the monolithic specimen with 1.0 m beam length, opening values reached approximately 7 mm, while shortening values were negligible (see Fig. 19-a). For the precast specimen with 1.0 m beam length, the measured separations (negative values) were negligible (see Fig. 19-b). It can be inferred that pre-tensioned bolts remained in their elastic range, and hence the pretension force was not exceeded. On the other hand, some shortening (positive values) were measured for the precast specimen. This can be attributed to the small bending of the beam end-plate observed during the tests. Fig. 1-b shows the deformed shape of the beam end-plate. It should be noted that the separation measurement rods of the precast specimens were welded to the beam end-plate, and therefore, they rotated with the plate. This implies that the precast connections did not practically exhibit any separation between the plates at beam-column interface.

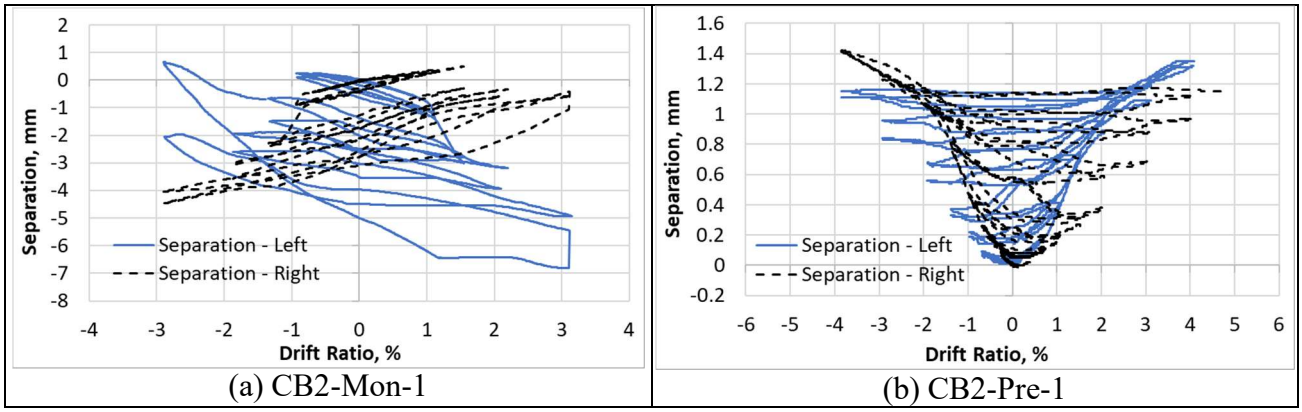

(a) CB2-Mon-1 (b) CB2-Pre-1

Fig. 19. Separation measurements at beam-column interface for CB2 specimens with 1.0 m beam

Fig. 20 represents the separation values measured for CB2 specimens with 2.0 m beam length (CB2-Mon-2, CB2-Pre-2). Unlike the CB2 monolithic specimen with 1.0 m beam length, both opening and shortening values (i.e. positive and negative separation) were observed for monolithic CB2 specimen with 2.0 m beam length. It is thought that this is the result of the bending moment dominant behaviour in this specimen. For precast CB2 specimen with 2.0 m beam length, similar to the CB2 specimen with 1.0 m beam length, the measures separations (negative values) were negligible compared to the shortening (positive values). The same justifications given for the CB2 specimen with 1.0 m beam length are valid here.

5.4. Failure Mode

Fig. 21 illustrates after-test views of the monolithic and precast CB1 specimens. The strain-gauge measurements indicate that the yielding of longitudinal rebar in the monolithic specimen started in an earlier stage of the loading compared to the precast connections (see Fig. 12). The failure mode of CB1 specimens was due to the flexural failure followed by shear failure. However,

the shear failure in the monolithic and precast specimens was observed at the panel zone and at the plastic hinge zone of the beam element, respectively. Although both specimens had the same detailing for column and beam elements, the anchorage system and the column surface plate used in the precast specimen increased the shear strength of the connection zone, leading to the change of the failure mechanism (see Fig. 5-b). This indicates that the proposed detailing for the precast connections not only increased the shear capacity of the connections but also shifted the damage to the beam element. This is in agreement with the concept of strong-column weak-beam that is recommended by seismic design guidelines. For better comparison, the failure modes of the tested specimens are listed in

Table 6.

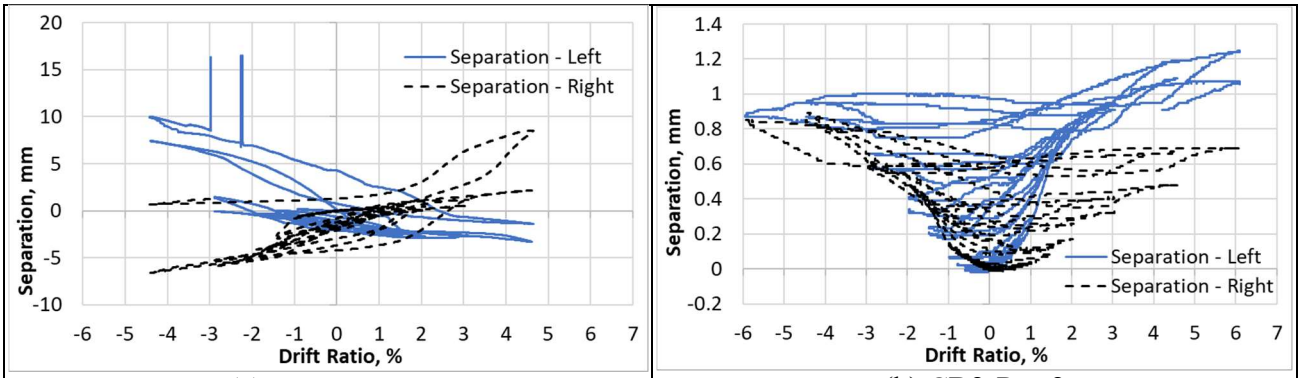

(a) CB2-Mon-2 (b) CB2-Pre-2

Fig. 20. Separations at beam-column interface for CB2 specimens with 2.0 m beam

(a) CB1-Mon-1 (b) CB1-Pre-1

Fig. 21. After-test view of CB1 test specimens

Fig. 22 shows close-up views of the failure zones of CB2 monolithic and precast specimens with 1.0 m beam length after the tests. For both specimens, the first flexural cracks were initiated at about 0.1% drift ratio. However, yielding of the longitudinal rebar in the precast specimen started at lower drift ratios compared to the monolithic one. At 1% drift ratio, the separation between concrete and steel plates started in the precast connection. At the same drift level, the first clear shear crack

occurred in the monolithic specimen. At this stage, the stiffness of the monolithic connection dropped dramatically, while the stiffness of the precast connection only slightly decreased until the first shear cracks appeared at 2% drift ratio. The monolithic and precast specimens reached the failure point at 3% and 4% drift ratio, respectively (see Fig. 13). Both CB2 monolithic and precast connections with 1.0 m beam length exhibited flexural cracking and yielding of longitudinal bars followed by shear failure at the plastic hinge zone of the beam elements.

It should be noticed that the main reason for the ultimate shear failure (after initiating the flexural cracks as discussed above) in CB1 and CB2 specimens with 1.0 m beam length was due to the high shear forces (compared to the bending moments) and decreasing the shear capacity of the concrete due to the flexural damage in the failure zone.

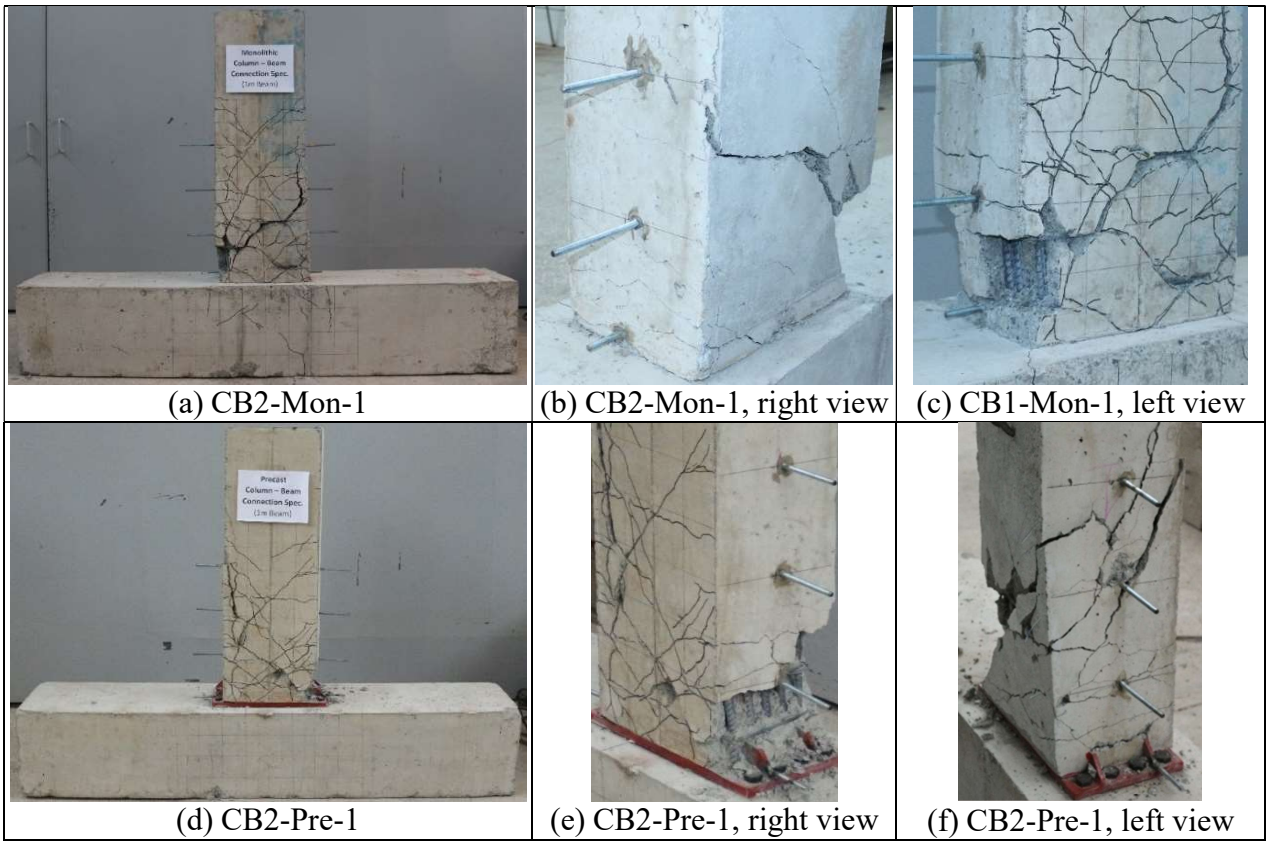

(a) CB2-Mon-1 (b) CB2-Mon-1, right view (c) CB1-Mon-1, left view

(d) CB2-Pre-1 (e) CB2-Pre-1, right view (f) CB2-Pre-1, left view

Fig. 22. After test views of CB2 specimens with 1.0 m beam length

Fig. 23 represents the after-test views of CB2 monolithic and precast specimens with 2.0 m beam length. For both of these specimens, the first flexural cracks were observed at 0.1% drift ratio. At 0.5% drift ratio, the separation between concrete and beam end-plate started in the precast connection, while rebars of monolithic specimen reached the yielding point. Subsequently, the first yielding at the longitudinal rebars of the precast specimen started at 1.0% drift ratio. For both specimens, cover spalling was observed at 3% drift ratio. The monolithic specimen (CB2-Mon-2) reached the failure point at 4.5% drift ratio, while the precast connection (CB2-Pre-2) exhibited a

satisfactory performance up to 6% drift ratio (see Fig. 14). The dominant failure mode for these specimens was due to flexural failure followed by buckling of the longitudinal rebar.

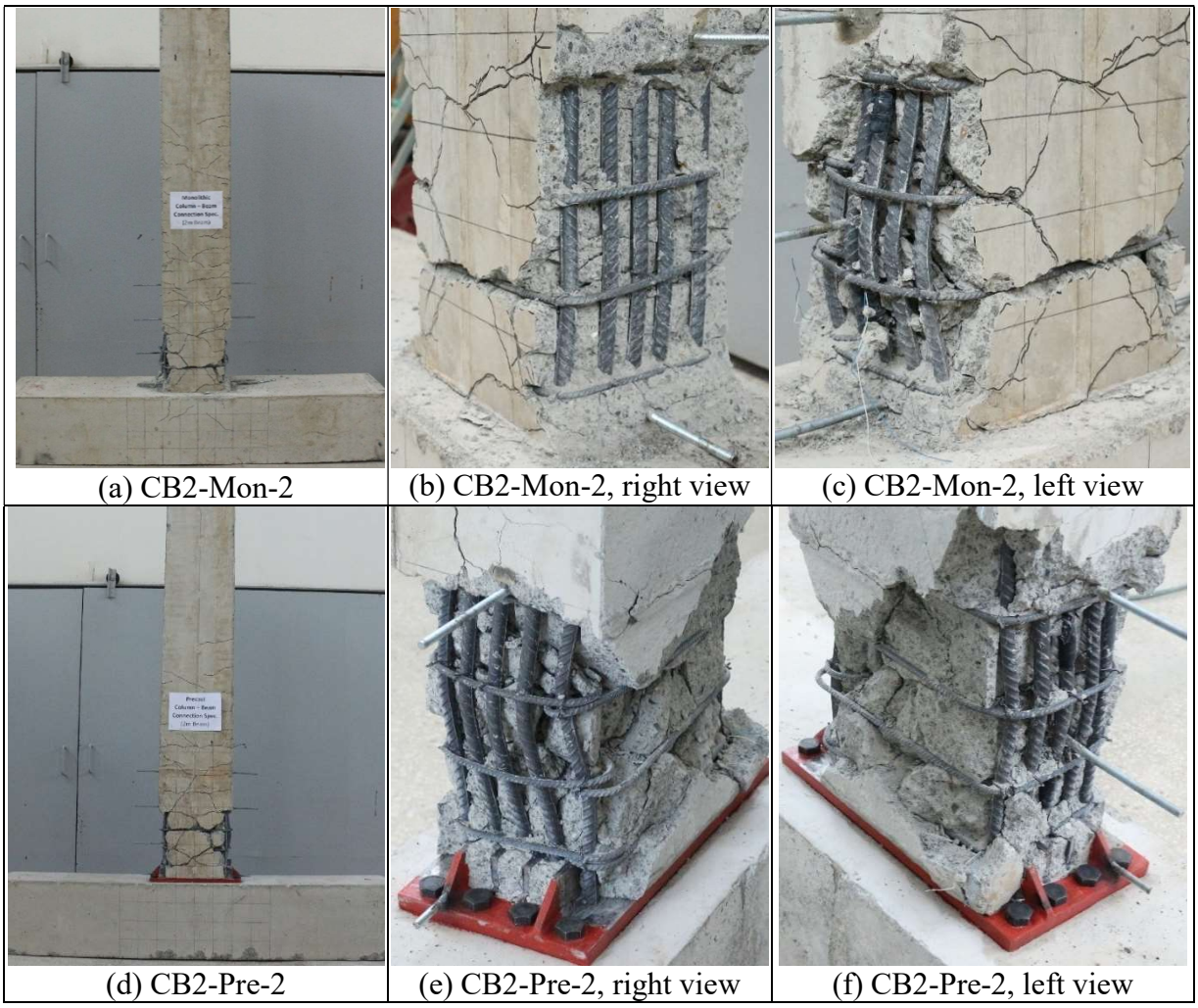

(a) CB2-Mon-2 (b) CB2-Mon-2, right view (c) CB2-Mon-2, left view

(d) CB2-Pre-2 (e) CB2-Pre-2, right view (f) CB2-Pre-2, left view

Fig. 23. After test views of CB2 specimens with 2.0 m beam length

5.4. Energy Dissipation

In general, the seismic performance of RC structures under strong earthquakes can be considerably improved by increasing the energy dissipation capacity of the elements and connections [33-37]. In this section, the energy dissipation capacity of the tested connections was obtained based on the area enclosed by their hysteresis curves. Fig. 24 shows the calculated energy dissipation capacity of the specimens for different drift ratios. The results indicate that, for the same drift ratio, monolithic connections exhibited slightly higher (on average 10%) energy dissipation. However, in most cases, the precast connections could dissipate higher energy levels at their ultimate points compared to their monolithic counterparts, due to their higher deformability (i.e. higher ultimate drift ratio).

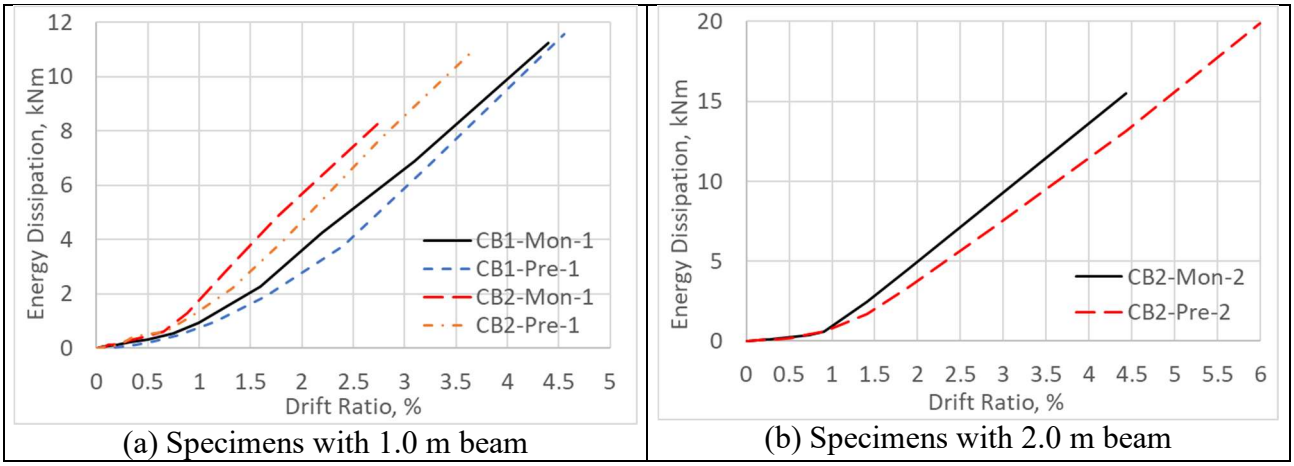

(a) Specimens with 1.0 m beam (b) Specimens with 2.0 m beam

Fig. 24. Dissipated energy

5.5. Ductility

To estimate the ductility of the specimens, ASCE/SEI 41-17 [32] approach is adopted in this study. The nonlinear force-displacement envelop curve of the referenced loading point (i.e. control node) is replaced with an idealized bilinear relationship to calculate the effective lateral stiffness, K_e, effective yield strength, V_y, and post-yield stiffness (αK_e) of the connection as shown in Fig. 25. The yield displacement (δ_y) is then determined based on the condition that the idealized bilinear curve intersects the actual force-displacement envelope curve at 60% of the nominal yield force (V_y), while the area under the bilinear and original curves up to the maximum displacement (δ_u) are equal. The ductility of the connections, μ, is then defined as the ratio of the maximum displacement (δ_u) to the calculated yield displacement (δ_y) of the connection.

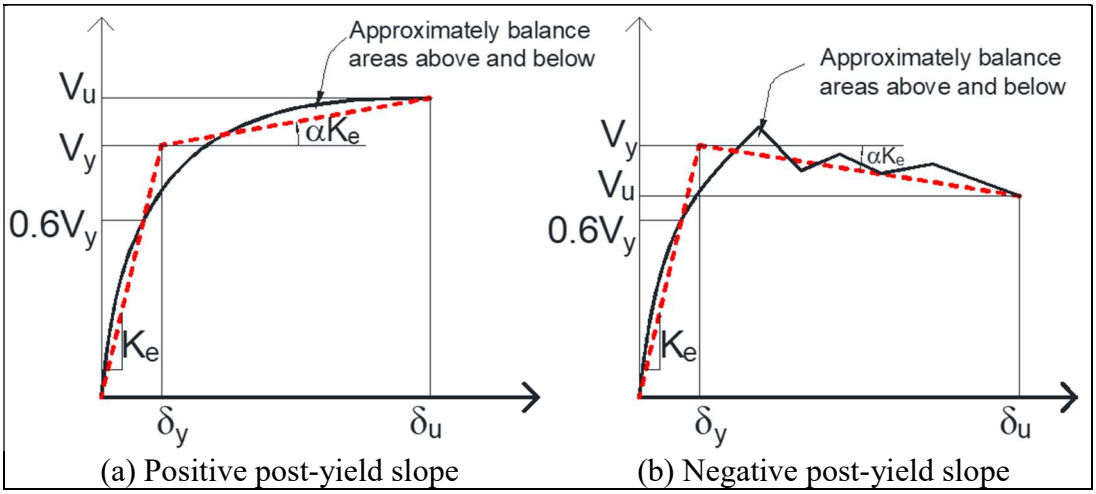

(a) Positive post-yield slope (b) Negative post-yield slope

Fig. 25. The idealization of the load-displacement curve (adopted from ASCE/SEI 41-17 [32])

Table 6 lists the maximum bending moment capacity, yield displacement, ultimate displacement and ductility of the monolithic and precast connections obtained from the idealized bilinear curves.

It is shown that CB2 precast connections exhibited higher (up to 24%) ductility compared to the similar monolithic connections. For CB1 specimens, however, the monolithic connection showed a higher ductility level mainly due to the different failure mechanism as discussed before. This highlights the importance of controlling the failure mode in the design of the precast connections.

In general, the results of this study indicate that the proposed precast connections (especially the detailing used for CB2 specimens) can provide higher or at least the same level of bending moment capacity, energy dissipation and ductility as monolithic connections, and therefore, can be efficiently used in precast concrete frames in seismic regions. It should be noted that it is not feasible to directly compare the response of the proposed precast connection system with the available data in the literature, since they use different detailing and working principles. However, in general, the results demonstrate the excellent seismic performance of the proposed precast connection compared to other conventional systems. For example, the cyclic behaviour curves (see Figs. 13 and 14) show that the proposed system exhibits considerably lower stiffness and strength degradation rates compared to the moment-resisting precast connection developed by Parastesh et al. (2014), while it generally leads to the same level of energy dissipation capacity (see Fig. 24) and ductility (see Table 6).

Table 6. Maximum bending capacity, yield displacement, ultimate displacement, ductility and failure modes of the tested connections

Specimen	Maximum bending capacity, kNm	Yield displacement, mm	Ultimate displacement, mm	Ductility	Failure mode
CB1-Mon-1	149.8	7.1	46.7	6.6	Flexural failure followed by shear failure at panel zone
CB1-Pre-1	181.5	9.9	43.3	4.4	Flexural failure followed by shear failure at plastic hinge zone of the beam
CB2-Mon-1	176.6	7.8	29.7	3.8	Flexural failure followed by shear failure at plastic hinge zone of the beam
CB2-Pre-1	185.4	8.2	38.4	4.7	Flexural failure followed by shear failure at plastic hinge zone of the beam
CB2-Mon-2	189.8	18.0	92.2	4.9	Flexural failure followed by longitudinal bar buckling
CB2-Pre-2	185.1	22.3	121.5	5.4	Flexural failure followed by longitudinal bar buckling

6. Finite Element Analyses

To perform analytical studies, detailed non-linear finite element (FE) models were developed in ABAQUS [38] finite element analysis software using “explicit dynamic” analysis procedure, which is suitable for complicated contact conditions such as those in precast connections. The models were subjected to constant axial load and monotonically increasing top displacement. The following sections present the details of the developed models and the accuracy of the predicted responses compared to the experimental test results.

6.1. Element type, geometry and boundary conditions

In this study, concrete and plate components were modelled using 3D solid elements (8-node hexahedron shaped C3D8R) with reduced integration, while the response of both longitudinal and transverse rebars was represented by 2-node beam elements (B31). Based on the results of a sensitivity analyses, the mesh size of 25 mm was found to provide a balance between accuracy of computational efficiency. To prevent irregular mesh shapes, concrete and plate geometries were portioned to have prismatic shapes. To model the hinge support, reference points were defined at the same section of the hinges and were tied to the column end by using multi point constraint (MPC) beam connectors. For the vertical boundary condition, the top and the bottom surfaces of the column were partitioned and the vertical constraints were defined at the exact position according to the experimental test setup. Fig. 26-a shows the finite element mesh and boundary conditions for CB2-Pre-1 specimen, while Fig. 26-b represents the reinforcement and plate details of the precast connection in the finite element model. It is shown that both transverse and longitudinal rebars were modelled in 3D space as beam elements. For the connection between the longitudinal rebars and the beam end-plate, MPC beam connectors were utilized. Connection plates were modelled as 3D specimens based on the geometries used in the experimental study (see Fig. 26-b). To simulate the behaviour of the bolted connections between the plates, MPC beam connectors were defined in the locations of the bolts. Also, a surface-to-surface hard contact was defined between the beam end-plate and column surface plate to transfer the compression loads. For the anchorage of the column surface plate, since there was no observed separation between column and the surface plate, a perfect bond was assumed between these elements.

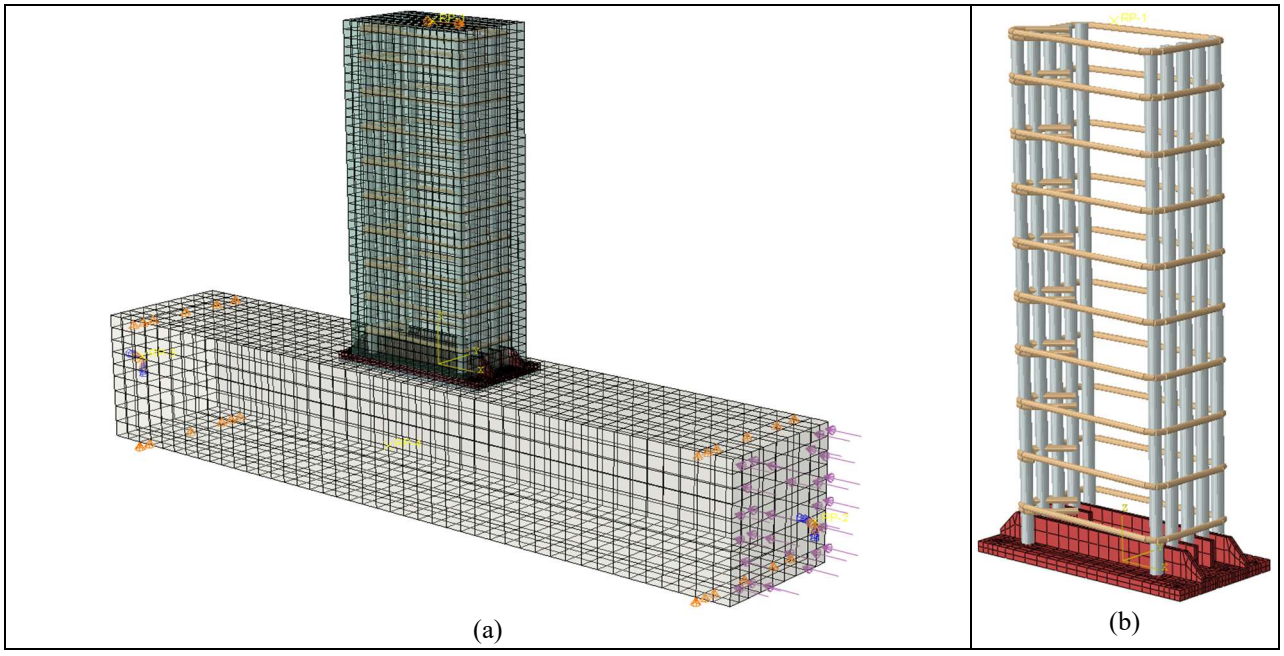

Fig. 26. (a) General view of CB2-Pre-1 model with load and boundary conditions (transparent); (b) Reinforcement cage system with beam end-plate

6.2. Material Modelling

6.2.1. Concrete material model

For the concrete material modelling, an elastoplastic damage model suggested by Krätzig and Pölling [39] for reinforced concrete was adopted, using the average cylinder concrete compressive strength of 42.7 MPa obtained from laboratory tests. To evaluate the strain at peak compressive strength, tensile strength, initial modulus of elasticity and fracture energy, CEB-FIP Model Code 1999 [40] was utilized. The model parameters were then calibrated using experimental test results. Fig. 27 shows the compressive and tensile behaviour curves used in the FE models. The inelastic parts of these curves were defined as the uniaxial hardening/softening parameters in the ABAQUS software [38].

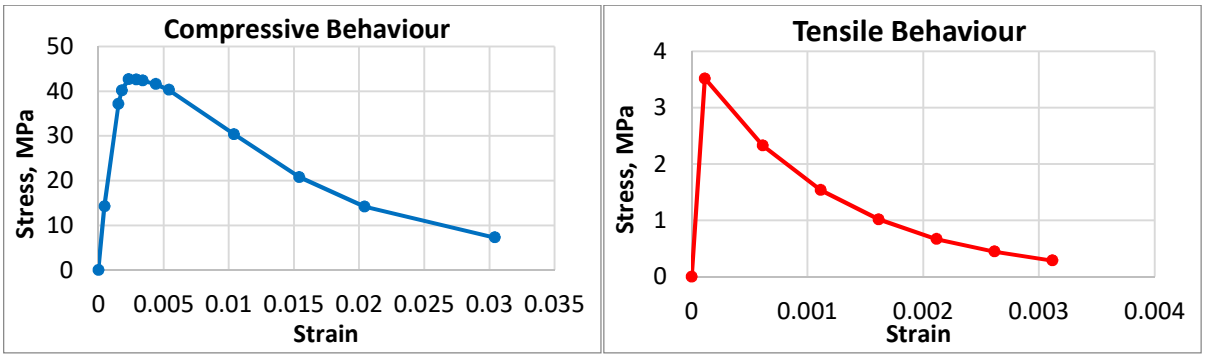

Fig. 27. Compressive and tensile behaviour of concrete material for finite element analyses

6.2.2. Steel material models for reinforcement and plates

To model steel material, Von-Mises plasticity model was adopted in this study. Reinforcement steel was defined as a trilinear model using the yield stress (491 MPa) and ultimate stress (618 MPa) values obtained from the material tests (see Fig. 8). For steel plates, a bilinear model was used based on the theoretical yield stress values for S235 grade steel (modulus of elasticity and yield stress of 200 GPa and 235 MPa, respectively).

6.3. Validation of Finite Element models

Using the briefly explained modelling approach, four detailed FE models corresponding to the CB2 monolithic and precast connections were created and analysed.

Fig. 28 and

Fig. 29 show the comparison of the FE predictions under monotonic loading with the experimental results for the CB2 specimens with 1.0 m and 2.0 m beam length, respectively. The comparison shows that the FE results could accurately predict the overall structural performance of both monolithic and precast connections in terms of initial stiffness, lateral load-bearing capacity and post peak behaviour. Therefore, these models should prove useful in the design and assessment of the proposed precast connection system. In can be noted that the monotonic FE responses did not show the significant strength degradation observed in the last load cycle of the experimental tests in CP2 precast connections. The main reason is the limitation of the developed FE models in capturing the failure mechanism of these specimens, which was due to shear failure for the specimen with 1.0 m beam length and longitudinal reinforcement buckling after cover spalling for the specimen with 2.0 m beam length. This is a topic for further investigation by the authors.

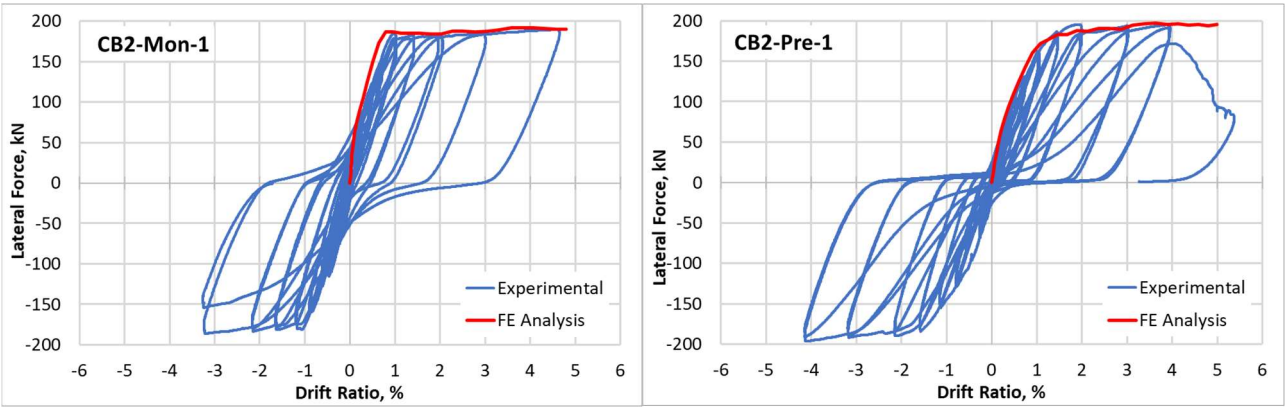

Fig. 28. Comparison of the experimental and FE results for CB2 specimens with 1.0 m beam length

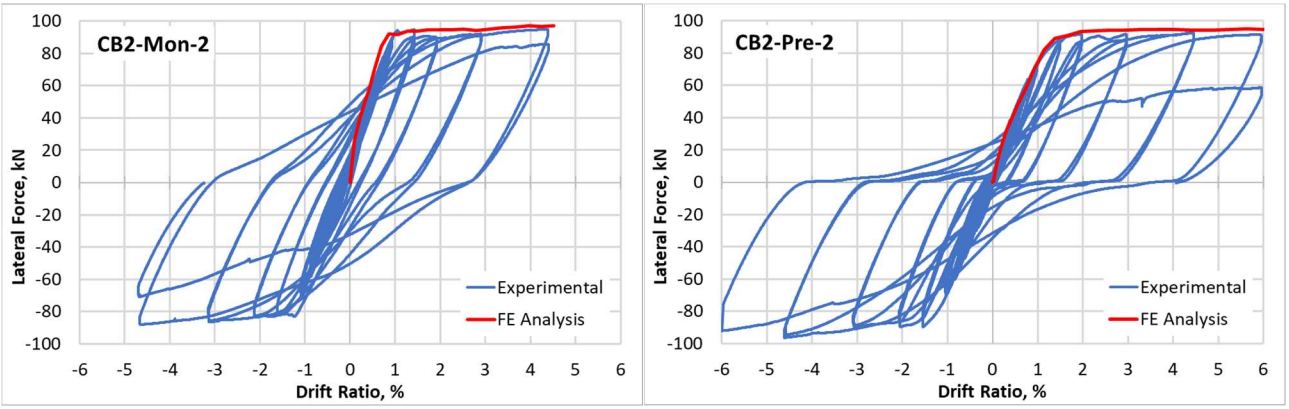

Fig. 29. Comparison of the experimental and FE results for CB2 specimens with 2.0 m beam length

7. Summary and Conclusions

A novel monolithic-like bolted moment connection system was developed for precast beam-column joints of RC frame structures in seismic regions, which offers several advantages such as rapid assembly and disassembly, reusability, and being replaceable if damaged during an earthquake event. Experimental tests were conducted on six full-scale precast and monolithic beam-column connections with different reinforcement ratios, specimen dimensions and detailing under displacement controlled cyclic loading. The cyclic behaviour, curvature distribution, failure mode, energy dissipation capacity and ductility of the specimens were obtained. Companion detailed non-linear finite element (FE) models were then developed using ABAQUS. Based on the results of this study, the following conclusions can be drawn:

1. The proposed precast connections exhibited considerably higher (up to 34%) ductility and ultimate drift ratio (deformability) compared to the similar monolithic connections, while they provided the same level of load-bearing capacity and initial stiffness. In the proposed connection system, the localized damage was also prevented by distributing the plastic deformations throughout the beam element.
2. The proposed precast connections, in general, dissipated higher energy levels up to their failure points compared to their monolithic counterparts. The precast connections with CB2 detailing also exhibited up to 24% higher ductility. By using CB1 detailing, however, the ductility was slightly reduced mainly due to changes in failure mechanism.
3. The experimental results showed that the column plate and the anchorage rods used in the proposed connection system could increase the shear capacity of the connection zone and shift the damage to the beam element, complying with the strong-column weak-beam design concept in seismic design guidelines.
4. The proposed monolithic-like precast connections could satisfy the ACI 318-14 [31] criteria to achieve at least 3.5% drift ratio with less than 25% loss in their load-bearing capacity. The precast connections could also reach the Collapse Prevention (CP) seismic performance level in accordance with ASCE 41-17 [32] without extensive damage. This implies that the proposed connection system is suitable for RC structures in seismic regions.
5. It was shown that the developed detailed FE models could accurately predict the overal structural performance of both monolithic and precast connections in terms of initial stiffness, lateral load-bearing capacity and post peak behaviour. However, the models could not capture the precise failure mechanism of the precast connections.

Acknowledgement

This study was supported by the Scientific and Technological Research Council of Turkey (TÜBİTAK), Grant No: 117M346.

References

[1] Elliott, K.S., 2016. *Precast concrete structures*. Crc Press.

[2] Polat, G., 2010. Precast concrete systems in developing vs. industrialized countries. *Journal of Civil Engineering and Management*, *16*(1), pp.85-94.

[3] Hamill, P., Bertolini, M., Biebighauser, M., Bechara, C.H. and Wilden, H., 2006. Precast concrete value engineering accommodates difficult site. *PCI journal*, *51*(4), p.18.

[4] Kazaz, A., Manisali, E. and Ulubeyli, S., 2008. Effect of basic motivational factors on construction workforce productivity in Turkey. *Journal of civil engineering and management*, *14*(2), pp.95-106.

[5] Nanyam, V.N., Basu, R., Sawhney, A., Vikram, H. and Lodha, G., 2017. Implementation of Precast Technology in India–Opportunities and Challenges. *Procedia engineering*, *196*, pp.144-151.

[6] Dineshkumar, N. and Kathirvel, P., 2015. Comparative study on prefabrication construction with cast in-situ construction of residential buildings. *International Journal of Innovative Science, Engineering & Technology (January 2015)*, pp.527-532.

[7] Iswahyudi, B.E., Azis, S. and Santosa, A.A., 2017. Analysis of Contruction Cost Efficiency Between Precast Method and Conventional Method in Building Project. *International Journal of Technology and Sciences*, *1*(1).

[8] Lachimpadi, S.K., Pereira, J.J., Taha, M.R. and Mokhtar, M., 2012. Construction waste minimisation comparing conventional and precast construction (Mixed System and IBS) methods in high-rise buildings: A Malaysia case study. *Resources, Conservation and Recycling*, *68*, pp.96-103.

[9] Korkmaz, H.H. and Tankut, T., 2005. Performance of a precast concrete beam-to-beam connection subject to reversed cyclic loading. *Engineering Structures*, *27*(9), pp.1392-1407.

[10] Kim, T.H., Lee, H.M., Kim, Y.J. and Shin, H.M., 2010. Performance assessment of precast concrete segmental bridge columns with a shear resistant connecting structure. *Engineering Structures*, *32*(5), pp.1292-1303.

[11] Wang, Z., Qu, H., Li, T., Wei, H., Wang, H., Duan, H. and Jiang, H., 2018. Quasi-static cyclic tests of precast bridge columns with different connection details for high seismic zones. *Engineering Structures*, *158*, pp.13-27.

[12] Alcocer, S.M., Carranza, R., Perez-Navarrete, D. and Martinez, R., 2002. Seismic tests of beam-to-column connections in a precast concrete frame. PCI journal, 47(3), pp.70-89.

[13] Ozturan, T., Ozden, S. and Ertas, O., 2006. Ductile connections in precast concrete moment resisting frames. *concrete construction*, *9*, p.11.

[14] Zhou, B., Wu, R., Feng, J., 2017. Two models for evaluating the bond behavior in pre- and post-yield phases of reinforced concrete. *Construction and Building Materials,* 30, pp. 847-857.

[15] Chen, Y., Sareh, P., Feng, J., Sun, Q., 2017, A computational method for automated detection of engineering structures with cyclic symmetries. *Computers & Structures,* 191, pp. 153-164.

[16] French, C.W., Hafner, M. and Jayashankar, V., 1989. Connections between precast elements—failure within connection region. Journal of Structural Engineering, 115(12), pp.3171-3192.

[17] Vidjeapriya, R. and Jaya, K.P., 2012. Experimental study on two simple mechanical precast beam-column connections under reverse cyclic loading. Journal of Performance of Constructed Facilities, 27(4), pp.402-414.

[18] Li, B., Kulkarni, S.A. and Leong, C.L., 2009. Seismic performance of precast hybrid-steel concrete connections. *Journal of Earthquake Engineering*, *13*(5), pp.667-689.

[19] Englekirk, R.E., 1995. Development and testing of a ductile connector for assembling precast concrete beams and columns. *PCI journal*, *40*(2), pp.36-51.

[20] Englekirk, R.E., 1996. An innovative design solution for precast prestressed concrete buildings in high seismic zones. *PCI journal*, *41*(4), pp.44-53.

[21] Dal Lago, B., Negro, P. and Dal Lago, A., 2018. Seismic design and performance of dry-assembled precast structures with adaptable joints. Soil Dynamics and Earthquake Engineering, 106, pp.182-195.

[22] Choi, H.K., Choi, Y.C., Choi, C.S., 2013, Development and testing of precast concrete beam-to-column connections. *Engineering Structures,* 56, pp. 1820-1835. --→ 23

[23] Parastesh, H., Hajirasouliha, I. and Ramezani, R. 2014. A new ductile moment-resisting connection for precast concrete frames in seismic regions: an experimental investigation. *Engineering Structures*, *70*, pp.144-157.

[24] Ozden, S. and Ertas, O., 2007. Behavior of unbonded, post-tensioned, precast concrete connections with different percentages of mild steel reinforcement. *PCI journal*, *52*(2).

[25] Aninthaneni, P.K. and Dhakal, R.P., 2017. Demountable Precast Concrete Frame–Building System for Seismic Regions: Conceptual Development. *Journal of Architectural Engineering*, *23*(4), p.04017024.

[26] Nzabonimpa, J.D. and Hong, W.K., 2018. Structural performance of detachable precast composite column joints with mechanical metal plates. *Engineering Structures*, *160*, pp.366-382.

[27] Chen, Y., Zhang, Q., Feng, J., Zhang, Z., 2019, Experimental Study on Shear Resistance of Precast RC Shear Walls with Novel Bundled Connections. *Journal of Earthquake and Tsunami,* 13, pp. 1940002.

[28] Tang, T., Shah, S.P. and Ouyang, C., 1992. Fracture mechanics and size effect of concrete in tension. *Journal of Structural Engineering*, *118*(11), pp.3169-3185.

[29] FEMA, 2007. Interim protocols for determining seismic performance characteristics of structural and nonstructural components through laboratory testing. *FEMA 461*.

[30] Park, R., 1989. Evaluation of ductility of structures and structural assemblages from laboratory testing. *Bulletin of the New Zealand national society for earthquake engineering*, *22*(3), pp.155-166.

[31] American Concrete Institute, 2014. *Building Code Requirements for Structural Concrete (ACI 318-14): Commentary on Building Code Requirements for Structural Concrete (ACI 318R-14): an ACI Report*. American Concrete Institute. ACI.

[32] American Society of Civil Engineers, 2017. Seismic Evaluation and Retrofit of Existing Buildings: ASCE/SEI, 41-17. American Society of Civil Engineers.

[33] Nabid, N., Hajirasouliha, I. and Petkovski, M., 2017. A practical method for optimum seismic design of friction wall dampers. *Earthquake Spectra*, *33*(3), pp.1033-1052.

[34] Zheng, Z., Pan, X. and Bao, X., 2018. Comparative Capacity Assessment of CFRP Retrofit Techniques for RC Frames with Masonry Infills Using Pushover Analysis. *Arabian Journal for Science and Engineering*, pp.1-16.

[35] Nabid, N., Hajirasouliha, I., Petkovski, M., 2018. Performance-based optimisation of RC frames with friction wall dampers using a low-cost optimisation method. *Bulletin of Earthquake Engineering*, 16(10), pp. 5017-5040.

[36] Cao, X.Y., Feng, D.C. and Wu, G., 2019. Seismic performance upgrade of RC frame buildings using precast bolt-connected steel-plate reinforced concrete frame-braces. *Engineering Structures*, *195*, pp.382-399.

[37] Nabid, N., Hajirasouliha, I., Petkovski, M., 2019, Adaptive low computational cost optimisation method for performance-based seismic design of friction dampers. *Engineering Structures*, 198, pp. 109549.

[38] Abaqus/CAE User's Guide, USA, 2016.

[39] Krätzig WB, Pölling R. An elasto-plastic damage model for reinforced concrete with minimum number of material parameters. Comput Struct 2004.

[40] CEB-FIP, M., 1993. 90. Design of concrete structures. CEB-FIP-Model-Code 1990. *British Standard Institution, London*.